Biophysical Journal Volume 76 April 1999 1951–1958

Chloride Ion Binding to Bacteriorhodopsin at Low pH: An Infrared Spectroscopic Study

Lóránd Kelemen, Péter Galajda, Sándor Száraz, and Pál Ormos
Institute of Biophysics, Biological Research Center of the Hungarian Academy of Sciences, Szeged, H-6701 Hungary

ABSTRACT Bacteriorhodopsin (bR) and halorhodopsin (hR) are light-induced ion pumps in the cell membrane of *Halobacterium salinarium*. Under normal conditions bR is an outward proton transporter, whereas hR is an inward Cl^- transporter. There is strong evidence that at very low pH and in the presence of Cl^-, bR transports Cl^- ions into the cell, similarly to hR. The chloride pumping activity of bR is connected to the so-called acid purple state. To account for the observed effects in bR a tentative complex counterion was suggested for the protonated Schiff base of the retinal chromophore. It would consist of three charged residues: Asp-85, Asp-212, and Arg-82. This quadruplet (including the Schiff base) would also serve as a Cl^- binding site at low pH. We used Fourier transform infrared difference spectroscopy to study the structural changes during the transitions between the normal, acid blue, and acid purple states. Asp-85 and Asp-212 were shown to participate in the transitions. During the normal-to-acid blue transition, Asp-85 protonates. When the pH is further lowered in the presence of Cl^-, Cl^- binds and Asp-212 also protonates. The binding of Cl^- and the protonation of Asp-212 occur simultaneously, but take place only when Asp-85 is already protonated. It is suggested that HCl is taken up in undissociated form in exchange for a neutral water molecule.

INTRODUCTION

The plasma membrane of *Halobacterium salinarium* contains several retinal proteins. Two of them, bacteriorhodopsin (bR) and halorhodopsin (hR), serve as light-driven ion pumps. Both of them are intrinsic membrane proteins with largely similar structure: both are a complex of an all-*trans* retinal and an opsin with homologous sequence and structure. Their specific functions, however, are different. bR is a light-driven proton pump; upon light absorption it transports protons across the cell membrane outside the cell. On the other hand, hR pumps chloride ions (Cl^-) in the opposite direction, into the cell, upon light excitation. Questions of what are the important functional differences between these two proteins and what structural details cause the large differences in their functions have been intensively studied.

In hR two arginine residues are assumed to be Cl^- binding sites (Lányi et al., 1988; Oesterhelt and Tittor, 1989). Although bR also has two arginine residues in similar positions, their inability to bind Cl^- ions has been suggested to originate either in the low pK of these side chains or in some nearby negatively charged group hindering their Cl^- binding (Oesterhelt and Tittor, 1989).

It has been observed earlier that upon lowering the pH, bR undergoes characteristic changes. First, with a pK of about 2.5 its absorption shifts to 605 nm and the acid blue form (bR_{AB}) is formed (Oesterhelt and Stoeckenius, 1971; Mowery et al., 1979). If the pH is further lowered in the presence of Cl^- or other halide ions the original color is regained and the acid purple state (bR_{AP}) is formed (Fischer and Oesterhelt, 1979). This form has been suggested to bind the Cl^- ion near the retinal binding site (Renthal et al., 1990).

Because, according to the logic of the comparison of the Cl^- binding ability of the arginine residues (Oesterhelt and Tittor, 1989) in bR and hR, the difference should vanish at low pH (by protonating either the low pK arginines or another nearby negative ion), Dér and co-workers raised the question whether bR_{AP} is capable of transporting Cl^-. Indeed, they have shown that when forming the acid purple form from the acid blue state, ion transport is regained (Dér et al., 1989). Although technical difficulties due to very low pH precluded explicit proof, all indirect tests were consistent with the assumption that the transported ion is Cl^-. Later, additional control experiments were performed, providing more circumstantial evidence (Keszthelyi et al., 1990; Dér et al., 1991).

When in bR, based on the analogous idea Asp-85 was exchanged for threonine with a much higher pK value, Cl^- transport could be directly demonstrated. It was already possible to measure this at normal pH values (Sasaki et al., 1995).

Although it has been questioned whether the acid purple form of bR exhibits any ion pumping activity (Moltke and Heyn, 1995), recent independent experiments reliably confirmed the original results (Kalaidzidis and Kaulen, 1997).

The paper by Dér et al. (1991) tentatively suggested a structure for the retinal binding site that could explain the basic differences between the normal, acid blue, and acid purple states. In this picture the counterion of the protonated Schiff base of the retinal binding site is a complex of three additional side chains, Asp-85, Asp-212, and Arg-82. This complex counterion would also provide the Cl^- binding site: in the normal and acid blue states a water molecule,

Received for publication 8 June 1998 and in final form 11 November 1998.
Address reprint requests to Dr. Pal Ormos, Institute of Biophysics, Box 521, Biological Research Center of the Hungarian Academy of Sciences, Temesvari krt. 62/ H-6701 Szeged, Hungary. Tel.: 36-62-433465; Fax: 36-62-433133; E-mail: pali@everx.szbk.u-szeged.hu.

0006-3495/99/04/1951/08 $2.00

whereas in the acid purple state a Cl^- ion neutralizes the positive charge on the other side chains.

In this work we performed titration experiments to test the validity of this suggestion. We used Fourier Transform Infrared (FTIR) spectroscopy to determine changes between the normal, acid blue, and acid purple states of bR to characterize the retinal binding site in these three characteristic states.

MATERIALS AND METHODS

Instrumentation

Infrared spectra were recorded on a Bruker IFS 66S Fourier transform infrared spectrometer (Bruker Analytical Instruments, Karlsruhe, Germany) equipped with a standard DTGS detector and an external horizontal attenuated total reflection (ATR) sample holder (Spectratech, Stamford, CT). This accessory includes a 45° trapezoidal germanium crystal and is designed for liquids.

FT-Raman spectra were collected on the same spectrometer equipped with the FRA-106 Raman attachment (Bruker Analytical Instruments). Excitation in this instrument is achieved with a diode-pumped NdYAG laser (wavelength = 1066 nm).

A Shimadzu UV-160 spectrophotometer was used to measure the absorption spectra in the visible spectral region (Shimadzu Corporation, Kyoto, Japan).

Sample preparation

Purple membranes were isolated from *H. salinarium* strain S9 according to Oesterhelt and Stoeckenius (1974). The D85T protein was expressed in *H. salinarium* strain Pho81, which lacks all other bacterial opsins (Sasaki et al., 1995).

Sample preparation for the infrared measurements was the same as described in detail in Száraz et al. (1994). bR was first dried on the surface of the Ge crystal of the ATR cell and subsequently covered with the appropriate solution. Titration was achieved by exchanging the solution above the sample; because the sample was not touched during these procedures, the changes induced by modification of the bathing solution could be detected with very high sensitivity and accuracy. The solutions used to cover the bR film on top of the Ge crystal were combinations of HCl, NaCl, and H_2SO_4. The actual concentration of the particular components varied according to the desired pH or ion concentration. The pH of the solvent was always set by the appropriate HCl or H_2SO_4 concentration; no additional buffer was used. By using this method we avoided the disturbing effect of the infrared spectra of additional buffers. Because between 1000 and 1300 cm^{-1} there are very intense vibrations of the SO_4 group masking the fingerprint region, only the spectra above 1300 cm^{-1} could be evaluated. To rule out the possible effect of pH dependence on light adaptation, single beam spectra (250 double-sided, forward-backward scans, 2 cm^{-1} resolution) were taken at ambient light intensity where the sample was dark-adapted.

For the FT-Raman measurements purple membranes were embedded in 6% polyacrylamide gel (2 mm thick). This gel was attached to the front side of a 5-mm quartz cuvette that had a reflective coating on its back. The cuvette was then filled with the solution according to the particular titration experiment. When changing the bathing solution, the gel was removed from the cuvette and soaked in a large access volume of the new solution overnight to achieve complete and proper exchange.

We observed solvent effects in the infrared and Raman spectra. Therefore we also performed control measurements with the bathing solution and, only after appropriate scaling, subtracted this background to minimize the solvent bands.

Data processing

Infrared difference absorption spectra were calculated according to the equation $\Delta A_x = -\log_{10}(I_x/I_{ref})$, where I_{ref} and I_x are single beam spectra, I_{ref} is the selected reference spectrum, and x indicates pH or chloride concentration.

The difference spectra were fitted to a sum of Lorentzians. Because the titration experiments were expected to yield continuous changes in parameters common to all spectra, a global fit procedure was used. All spectra from a single titration experiment were fitted simultaneously, with the following coupling between the parameters: each curve was fit to the same number of Lorentzians, and the positions and widths of the corresponding Lorentzians were identical for each curve in the set. The amplitudes were allowed to be different from curve to curve. During the fit the common position and width values and the individual amplitude values were varied. The number of Lorentzians for the fit was determined by reasonable judgment: between 10 and 13 bands were necessary for a good description with sufficient detail in the regions discussed. In the protein bands certain fine structures (e.g., around 1500 cm^{-1} in Fig. 1 *b*) were ignored to prevent an escalation of the number of components. The fit procedure used the Levenberg-Marquardt least-squares minimization algorithm, performed with routines using the Matlab package (MathWorks, Inc., Natick, MA).

The resulting amplitudes of selected Lorentzians were used to determine pK_a values of the molecular transitions.

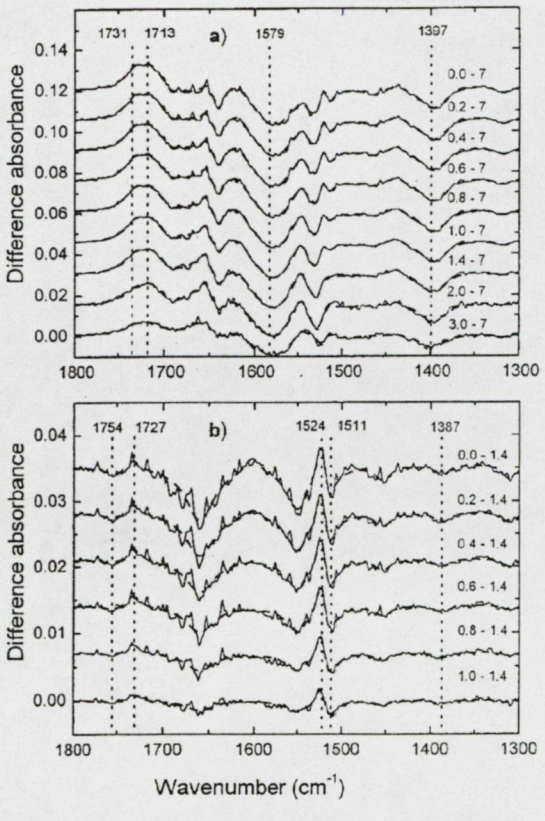

FIGURE 1 FTIR spectra measured during the acid titration of bR in the presence of 1M Cl^-. The solution contained 1M NaCl, the pH of the solution was set with 1 M HCl. The spectra reflect the difference induced by the pH change between the reference pH value and the pH value indicated in the curve. (*a*) Curves reflecting changes relative to pH = 7. (*b*) Curves reflecting changes relative to pH = 1.4. *Solid line*, measured data; *dashed line*, fit.

RESULTS

Our goal was to determine separately the effects of acidification and Cl^- binding. The procedure we applied to observe the two effects without permitting them to influence each other was based on the finding of Renthal et al. (1990) that acid and chloride effects can be separated using H_2SO_4. Two types of titration experiments were performed. First, acid titration was achieved at constant and saturating Cl^- concentration. Second, the effect of Cl^- was tested in a Cl^- titration experiment where proton concentration was kept at a saturating level: a constant pH of 0 was maintained while H_2SO_4 was exchanged for HCl. This approach was followed during the infrared, visible, and Raman measurements. During exchange of the solvent above the protein layer, in some cases, differences showed up due to changes in the sample thickness caused by the change of ionic composition or pH. These changes affected the amide regions and were not relevant in this study.

Investigation of the bR → bR_{AB} → bR_{AP} transition by acid titration in the presence of high Cl^- concentration

In the first series of measurements pH was lowered from 7 down to 0 by mixing appropriate amounts of 1 M HCl and 1 M NaCl (Fig. 1 *a*). According to Fischer and Oesterhelt (1979) and Váró and Lányi (1989), under these conditions both acidic states of bR form. Because the 1 M Cl^- concentration is high enough to saturate the Cl^- effect over the pH range where significant amount of bR_{AP} forms (Renthal et al., 1990), the transition is induced exclusively by the acidification of the bathing medium.

Fig. 1 *a* shows the series of infrared difference spectra obtained at different pH values. These spectra reflect changes in the structure relative to pH = 7. Although complete assignment of each band in this kind of spectra is not possible, we can make several firm assignments. For a review of the interpretation of infrared spectra of bR, see Rothschild (1992).

The protonated form of carboxylic acids has a characteristic frequency above 1680 cm^{-1} that originates from the $\nu_{C=O}$ bond stretch of the COOH group (Bellamy, 1980). In the bR difference spectra the region above 1700 cm^{-1} belongs exclusively to the COOH absorption; other vibrations can seldom reach such high frequencies. One possible source of ambiguity might be the $\nu_{C=O}$ mode of the ester group of lipids, but fortunately natural lipids in purple membrane do not have such esters (Stoeckenius et al., 1979). Consequently, we attribute the broad positive band above 1700 cm^{-1} (resolved to two Lorentzian bands centered at 1731 and 1713 cm^{-1}) to the protonation of several Asp or Glu side chains. The corresponding negative bands of disappearing COO^- are found at 1579 cm^{-1} and 1397 cm^{-1} (asymmetric and symmetric vibrations, respectively).

The change in the maxima of the visible absorption spectra due to the formation of the acidic forms is also reflected in the vibrational spectra as a shift of the frequency of the C = C vibration of the retinal chromophore (Aton et al., 1977). Raman spectroscopy can be used as a tool to separate bands associated with chromophore vibrations from those of the protein. To separate the characteristic bands of the chromophore in the different states, we measured FT-Raman spectra under conditions identical to those of the infrared measurements (Fig. 2). Results agree well with the resonance Raman spectra of Smith and Mathies (1985), although there are slight differences in peak positions and relative amplitudes, probably due to the near-infrared excitation used in our case (Sawatzki et al., 1990; Rath et al., 1993). According to the Raman data, we assigned the complex features of the infrared difference spectra depicted in Fig. 1 in the region of ~1510–1530 cm^{-1} to the ethylenic vibrations of the chromophore. In accordance with the literature (Smith and Mathies, 1985; de Groot et al., 1990), our Raman data indicate that chromophore bands not only shift during these transitions but also differ because of the altered retinal isomeric composition in the different acidic states. The Raman spectrum (Fig. 2) of bR clearly shows two overlapping bands, indicating that a mixture of 13-*cis* and all-*trans* retinal is present (full width at the half maximum (FWHM) is 22 cm^{-1}). In the bR_{AB} spectra only one band can be seen but, according to the relatively high 23 cm^{-1} FWHM of the band, it is reasonable to suppose this form to exist in dark-adapted form, too. In the bR_{AP} states only one band can be seen and its FWHM suggests that in this state, the sample is only in all-*trans* form. Due to this complexity, curve fitting to Lorentzians was not able to completely resolve the spectral changes in the ethylenic region of the infrared spectra in Fig. 1 *a* but performed very well under conditions where only the transition between bR_{AB} and bR_{AP} was observed (Fig. 1 *b* and Fig. 5).

The acidic forms of bR were originally identified by their visible absorption spectra (Fig. 3 *a*) therefore to support the

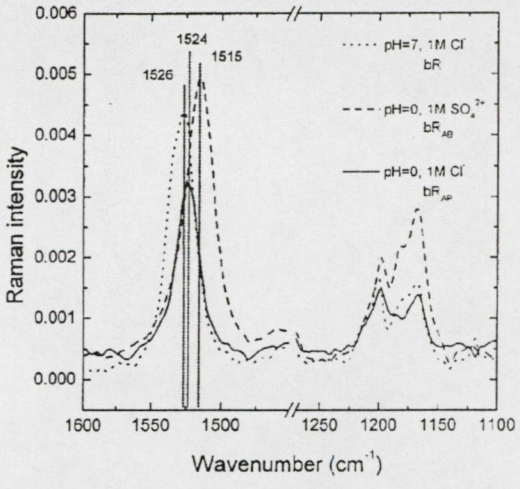

FIGURE 2 FT-Raman spectra measured in the bR, bR_{AB}, and bR_{AP} states. The actual H^+ and Cl^- concentrations were set by using 1 M HCl, 1 M H_2SO_4 and 1 M NaCl.

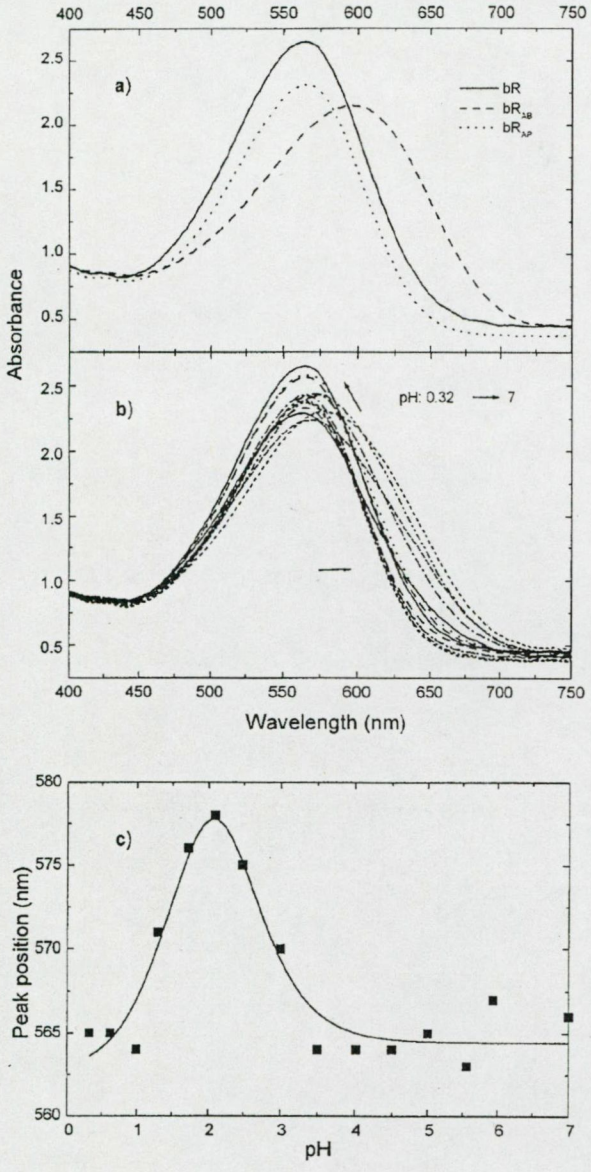

FIGURE 3 Visible spectroscopy of the acid titration of bR in the presence of 1M Cl^-. (*a*) The spectra of the characteristic states of bR (bR, bR_{AB}, and bR_{AP}). (*b*) The evolution of the spectra with changing pH. (*c*) The position of the absorption maxima as a function of pH. The solid line represents a fit to two pK values: $pK_1 = 2.3$ and $pK_2 = 1.33$.

infrared data we performed analogous experiments in the visible spectral region, too (Fig. 3 *b*). Under these conditions the data could be evaluated by assuming two pK_a values (Fig. 3 *c*). A global curve fitting to all amplitudes with Eq. 1 resulted in $pK_{a1} = 2.3$ and $pK_{a2} = 1.33$ for the $bR \rightarrow bR_{AB}$ and $bR_{AB} \rightarrow bR_{AP}$ transitions, respectively.

To derive pK_a values from the infrared data the difference spectra were first deconvoluted to a sum of Lorentzians by the global fit procedure (see Materials and Methods). The pH dependence of the amplitudes of the Lorentzians were then used to calculate the pK_a values ($pK_{a1} = 2.97$ and $pK_{a2} = 1.39$). For the $bR_{AB} \rightarrow bR_{AP}$ transition there is a good agreement between the titration experiments performed in the visible and in the infrared. However, for the $bR \rightarrow bR_{AB}$ transition, the titration followed in the infrared yields a significantly higher pK_a value. A reasonable explanation is given below for the difference.

On the spectra shown in Fig. 1 *a* it is apparent that the bands characteristic to carboxylic groups change considerably in the pH region between 3 and 1.4. It was shown previously that during the formation of bR_{AB} about 14 water-exposed carboxyl groups become protonated (Gerwert et al., 1987). Based on the pK_a values of carboxylic side chains of amino acids in solutions ($pK_a = 3.9$ for aspartic acid and $pK_a = 4.3$ for glutamic acid), the protonation of these groups would be expected to take place in a pH region higher than the range of our measurements. Moreover, based on the large relative size, broadness, and inhomogeneity of the bands in the 1750–1700 cm^{-1} spectral range and around 1390 cm^{-1}, we assigned these spectral changes to these water-accessible carboxylic groups of bR. According to our data about two-thirds of these surface groups get protonated only when $pH < 3$, coinciding with the pH range where the bR_{AB} transition occurs. In ^{13}C cross-correlation magic angle spinning (CP-MAS) NMR experiments Metz et al. (1992) found correlation between the color change during the $bR \rightarrow bR_{AB}$ transition and the protonation state of Asp-85: the purple-to-blue transition occurs parallel with the protonation of the negatively charged Asp-85 in the complex counterion of the Schiff base. Because this crucial protonation coincides with the protonation of several other carboxylic groups of the molecule, we were unable to separate the expected spectral changes that were unambiguously due to the proton uptake of only Asp-85; they were also not seen by Gerwert et al. (1987). This argument also explains why the pK value for the $bR \rightarrow bR_{AB}$ transitions obtained from the FTIR spectra is considerably higher than that obtained from the visible spectra. In the titration followed in the infrared the protonation of surface carboxylic groups with pK close to the bulk may also contribute, thus apparently shifting the pK of the transition to a higher value.

To reveal spectral changes attributed to the formation of bR_{AB} we have calculated difference spectra using the single beam spectrum measured at pH = 1.4 as the reference (Fig. 1 *b*). Because this value is close to the midpoint of the $bR_{AB} \rightarrow bR_{AP}$ transition, negative bands in these spectra are characteristic of those of bR_{AB}, whereas the positive ones are characteristic of those of bR_{AP}. This is confirmed by the appearance of a negative band at 1511 cm^{-1} that can be attributed to the ethylenic stretch of the bR_{AB} chromophore and a positive band at 1524 cm^{-1} due to bR_{AP}. In the FT-Raman spectra we have found the values of 1516 cm^{-1} and 1526 cm^{-1}, respectively (Fig. 2). In the region of the $\nu_{C=O}$ vibration of COOH groups we have found two bands, a negative one at 1754 cm^{-1} and a positive one at 1727 cm^{-1}. Note that the amplitude of the 1727 cm^{-1} band is

about twice that of the one seen at 1754 cm^{-1}. The appearance of a 1387-cm^{-1} negative band characteristic of a carboxylate anion indicates that an Asp or Glu residue having its carbonyl frequency at 1727 cm^{-1} became protonated during the transition. It is very unreasonable to suppose that a carboxyl group would deprotonate upon increasing proton concentration; consequently, we attribute the 1754 cm^{-1} negative band to the effect of Cl^- binding induced by the lowered pH.

Investigation of the $bR_{AB} \rightarrow bR_{AP}$ transition by Cl^- titration

In the second set of experiments proton concentration was kept at a constant value of ≈1 M (pH = 0) high enough to saturate proton binding. In this series of experiments, first pH = 0 was set by 1 M H_2SO_4 and this was gradually exchanged to 1 M HCl to increase Cl^- concentration. At the beginning of the experiment (in 1 M H_2SO_4) the pigment is in the bR_{AB} state but in 1 M HCl complete transition to the bR_{AP} state is reached (Renthal et al., 1990). As the proton concentration was kept constant in these experiments, the $bR_{AB} \rightarrow bR_{AP}$ transition was induced by Cl^- binding.

The result of these experiments is shown in Fig. 4. The ethylenic bands are similar to the ones in the spectra depicted in Fig. 1 *b* and clearly show that conversion from bR_{AB} (as indicated by the negative band at 1511 cm^{-1}) to bR_{AP} (as indicated by the positive band at 1521 cm^{-1}) occurs during the experiment. It is interesting to look at the bands characteristic of carboxylic groups. In the region of the carbonyl stretching vibrations of COOH groups we have obtained the same changes as in the acid titration: a negative band at 1752 cm^{-1} and a positive one at 1729 cm^{-1}. Here also, the 1729 cm^{-1} band has an amplitude twice that of the band at 1752 cm^{-1}. The negative band at 1389 cm^{-1} associated with the carboxylate anion is also present. This confirms that all of these spectral features are characteristic of the $bR_{AB} \rightarrow bR_{AP}$ transition and are not dependent on whether the transition was induced by acidification in the presence of Cl^- ions or by adding Cl^- ions at pH = 0.

To provide experimental data to further explore the origin of the carboxylic bands, we performed control experiments on the D85T mutant of bR. The structure of the complex counterion in this mutant is similar to hR and it was shown to bind and pump Cl^- ions even under physiological conditions (Sasaki et al., 1995). Fig. 6 shows the change of the infrared spectrum upon Cl^- binding at pH = 0.

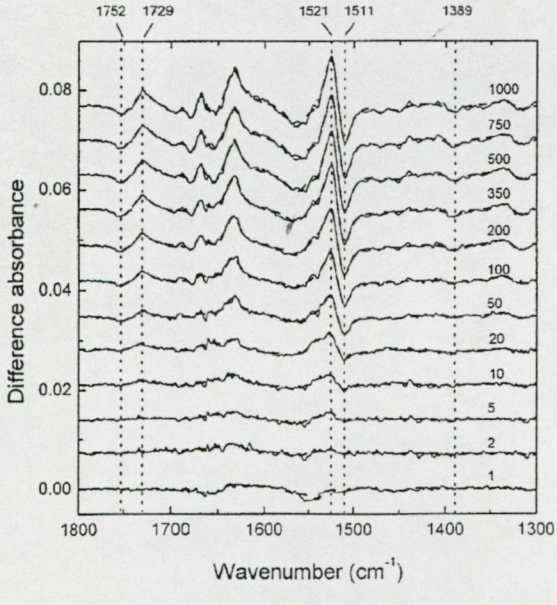

FIGURE 4 FTIR measurement of the Cl^- titration experiment. The pH of the solution was kept constant at pH = 0, while H_2SO_4 was exchanged to HCl. The spectra reflect the differences due to the exchange of SO_4^{2-} to Cl^- referenced to the state with only SO_4^{2-} to the Cl^- concentration marked above the curves. *Solid line*, measured data; *dashed line*, fit.

DISCUSSION

Assignment of spectral changes to individual groups of bR

The spectral changes in the region of the carboxylic vibrations show essentially the same features independent of whether the transition was induced by acidification in the presence of high Cl^- concentration or by addition of Cl^- ions at high proton concentration (Figs. 1 and 4). Similar spectral changes were also obtained in comparable experiments of other groups. Marrero and Rothschild (1987) investigated the structural changes associated with the formation of bR_{AB} in an experiment similar to ours. Because they used HCl to change pH, not only bR_{AB} but also bR_{AP} has been formed in their experiment. By using only HCl to set the pH, it is not possible to separate the effects of Cl^- binding and H^+ binding. Although their paper does not

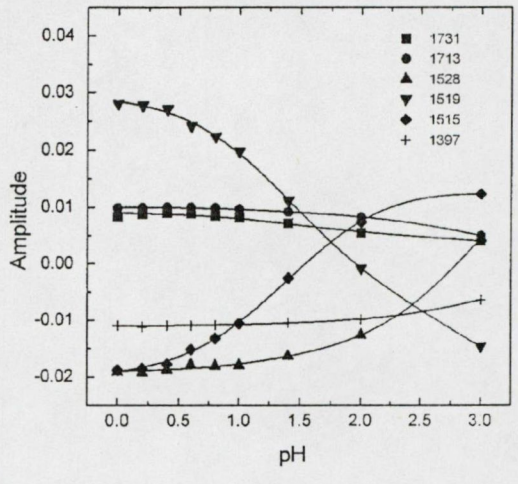

FIGURE 5 The change of the amplitudes of selected Lorentzians fitted to the infrared spectra during the acid titration experiment. The curves are the result of the global fit with two pK values, $pK_1 = 2.97$ and $pK_2 = 1.33$.

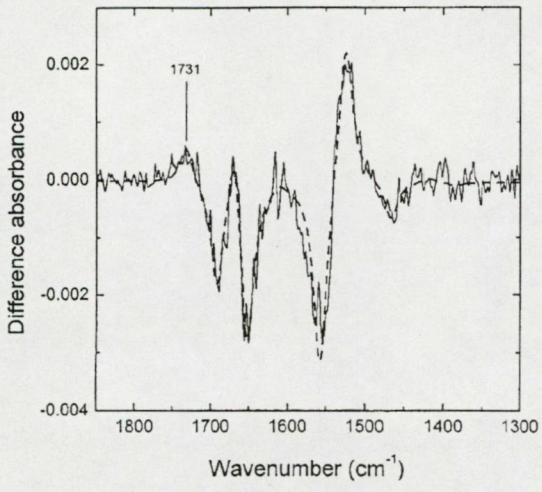

FIGURE 6 Difference spectra of bR mutant D85T between 0 and 1 M Cl^- at pH = 0. *Solid line*, measured data; *dashed line*, fit.

explicitly discuss it, if one compares the ethylenic and COOH bands with our data, the presence of bR_{AP} is apparent at low pH, e.g., in the pH = 1.8 to pH = 1.4 difference spectra, a negative ethylenic band demonstrates the loss of bR_{AB} (1509 cm^{-1}) and a positive one the formation of bR_{AP} (1524 cm^{-1}). In agreement with our data, there is a negative band at 1755 cm^{-1} and a positive one at 1732 cm^{-1}. The $bR_{AB} \rightarrow bR_{AP}$ transition was investigated by Le Coutre et al. (1995). In this investigation, the conversion to bR_{AP} was induced by blowing HCl gas onto a pellet of purple membranes originally in the acid blue state. The obtained peak positions were 1515 cm^{-1} and 1531 cm^{-1} for the ethylenic bands and 1762 and 1731 cm^{-1} for the negative and positive carboxylic bands, respectively. These features were essentially unchanged in the Arg-82 mutant. Based on the well known light-induced M-bR difference spectra (M is a photocycle intermediate), the negative band at 1762 cm^{-1} was attributed to Asp-85 and it was assumed to downshift to 1733 cm^{-1} upon Cl^- binding. A similarly high frequency, 1754 cm^{-1}, was suggested for Asp-85 by Masuda et al. (1995) from the study of deionized blue bR. Mitrovich et al. (1995) assigned the peak at 1732 cm^{-1} to Asp-85 in the bR_{AP} state by investigating the bR_{AP} photocycle on wild-type bR and mutants. Although the paper does not state this, its figures suggest that Asp-212 is protonated also in the bR_{AP} state and its frequency is around 1730 cm^{-1}. In contrast, Braiman et al. (1996) provided experimental evidence that the COOH band of Asp-85 in unphotolyzed bR is found at 1723 cm^{-1}. This conclusion was obtained from an experiment similar to ours, but the infrared difference spectrum was calculated only between two nearby pH values, close to the pK_a of the $bR \rightarrow bR_{AB}$ transition. Our data covering a much broader pH range clearly show that in the pH region where the formation of bR_{AB} from bR is observed, the COOH bands change much more than would be expected from the protonation of only one COOH band. We suggest that the big size and unusual broadness of the cited band is due to the protonation of a number of water-exposed carboxyl groups that protonate with a pK_a significantly lower than a typical aspartate or glutamate pK_a (≈4) in solution. A similar conclusion was drawn by Marrero and Rothschild (1987), who found that upon acidification of purple membranes most of the carboxyl protonation changes occur in the pH range between 3 and 2. As we have seen earlier, the higher pK_a value obtained from the fit to the data from the FTIR experiment for the $bR \rightarrow bR_{AB}$ transition also points to the fact that protonation of carboxyl groups not directly connected to the color change takes place in this pH region, which is higher than the actual transition but lower than the bulk value. Therefore, we believe that the broad 1723 cm^{-1} band belongs to these water-accessible groups.

The above arguments also explain why we could not separately observe the protonation of Asp-85 during the $bR \rightarrow bR_{AB}$ transition (Fig. 1). The large and inhomogeneous band that extends from 1690 cm^{-1} to 1760 cm^{-1} due to the several other water-accessible acidic groups masks the Asp-85 band as it extends over the frequency region where the COOH group of Asp-85 is also expected to appear. NMR data indicated a rather hydrophobic environment for Asp-85 both in the M state of the photocycle and in the ground state bR (Metz et al., 1992). The carbonyl frequency of a carboxyl group depends on the polarizability of the environment (Bellamy, 1980; Dioumaev and Braiman, 1995). This would favor assignment of the higher frequencies to Asp-85 close to the value observed in the M form.

The control experiments performed on the bR mutant D85T helped to identify the side chains with the carboxylic groups responsible for the observed changes during the binding of Cl^- (Fig. 6). Although due to the instability of the mutant sample under the measuring conditions the quality of this spectrum is not as good as in the case of wild-type bR, it is evident that the positive carboxyl band is preserved around 1730 cm^{-1} but the negative one at the higher frequency is missing. Assuming that Cl^- is bound by a similar mechanism to this mutant as it is to wild-type bR, the most obvious source of the band at 1731 cm^{-1} is Asp-212. Due to the instability of the mutant sample the Cl^- titration caused more expressed amide changes that can be followed clearly in the amide I and II regions. These amide bands are large enough to mask the shift in the C = C region that reflects the color change of the sample.

In conclusion, taking into account the arguments above and our results on the D85T mutant of bR, we attribute the negative carboxyl band at 1754 cm^{-1} (Fig. 1 *b*) and 1752 cm^{-1} (Fig. 4) to Asp-85 and the positive band at 1727 cm^{-1} (Fig. 1 *b*) and at 1729 cm^{-1} (Fig. 4) to Asp-212 and Asp-85. Using this identification, one can relate the observed spectral changes to the following molecular events. Based on the NMR experiments of de Groot et al. (1990), we attribute the positive carboxyl band found at 1730 cm^{-1} to the protonation of Asp-212. To explain that upon formation of bR_{AP} the

localization of the electric charges around the Schiff base is practically identical to that of bR, as it was concluded from the comparison of their visible absorption and Raman spectra (Smith and Mathies, 1985) and study of bR mutants (Marti et al., 1991), to substitute its negative charge in the bR_{AP} state the bound Cl^- ion must reside close to Asp-85. The appearance of the Cl^- anion close to the retinal binding site (highly apolar in the bR_{AB} state) induces changes in the region that probably include the appearance of one or more water molecules, or may involve H bonding to the COOH carbonyl. The increase of polarizability (dielectric constant) as well as H bonding result in a downshift of the carbonyl frequency (Dioumaev and Braiman, 1995) to approximately 1730 cm^{-1}, according to our data. This frequency shift explains the negative band at around 1750 cm^{-1} and the fact that the amplitude of the 1730 cm^{-1} band is about twice as large as the negative band at 1750 cm^{-1} (similar to the spectra of Le Coutre et al., 1995), i.e., at 1730 cm^{-1} the COOH vibration of both Asp-85 and Asp-212 in the bR_{AP} state is seen. The presence of the negative band at 1390 cm^{-1} (the loss of COO^-) confirms that protonation of a carboxylic group occurs upon formation of bR_{AP} and spectral changes cannot be explained only by the shift of the carbonyl band of a single protonated carboxyl group. It is also very improbable that anion binding itself would change the intensity of the carbonyl band to such an extent. Because, according to our data, Cl^- binding is negligible until most of bR is converted into bR_{AB} and significantly increases below the pK_a of this transition (the apparent dissociation constant is 1.5 M at pH = 2 but it goes down to 35 mM at pH = 0, according to Renthal et al. (1990)), we conclude that one of the prerequisites of halide anion binding is the protonation of Asp-85. It is more interesting to discuss the role of Asp-212. NMR measurements showed that only Asp-85 gets protonated in the absence of halide anions upon acidification; protonation of Asp-212 was observed exclusively in the bR_{AP} form (de Groot et al., 1990; Metz et al., 1992). Our data also show that acidification in the presence of Cl^- induces the protonation of Asp-212 along with the binding of the anion to the complex counterion as indicated by the ethylenic bands, but interestingly, protonation of Asp-212 also occurs if the pH is kept constant and sulfate anions are exchanged for Cl^-. This suggests that protonation of Asp-212 occurs in parallel with Cl^- binding, but only if Asp-85 is already protonated. Protonation of Asp-212 and Cl^- binding can apparently take place only simultaneously. We suggest therefore that Cl^- is picked up in the form of undissociated HCl (and an H_2O molecule is released in exchange) and dissociates inside the protein. The feasibility of such a reaction was shown in a molecular dynamics simulation of HCl ionization at the surface of stratospheric ice (Gertner and Hynes, 1996).

All of these findings confirm with independent experiments the validity of the model for the structure of the Schiff base counterion in the different acidic states introduced in Dér et al. (1991). NMR data (de Groot et al., 1990) support the theory that in the $bR_{AB} \rightarrow bR_{AP}$ transition, Cl^- is exchanged for an OH^- or H_2O is exchanged for dissociated HCl.

In the case of hR two anion binding sites were suggested (Lányi, 1990) and both were hypothetically assigned to positively charged arginine residues. In fact, it was shown that in the hR mutant R108Q the chloride transport was completely inactivated. In bR_{AP} the role of Arg-82 in Cl^- binding is not yet clear. The band that would indicate the perturbation of the guanidino group of Arg-82 by the bound Cl^- is expected between 1650 cm^{-1} and 1690 cm^{-1} (Braiman et al., 1994). The negative peak at 1690 cm^{-1} in Fig. 6 has an amplitude comparable to the amide change, so this is too large in both amplitude and width to be a reasonable candidate to represent the change of a single Arg peak. Unfortunately, in our case we have the poorest signal-to-noise ratio in the 1600–1700 cm^{-1} region due to the high water absorption in this region. In addition, the assignment of small bands is unreliable because of the overlap with the amide I band; consequently a reliable statement about the Arg side chain cannot be made. Le Coutre and co-workers (1995) found only very small influence of the replacement of Arg-82 by a lysine on the $bR_{AB} \rightarrow bR_{AP}$ transition and suggested that Arg-82 does not play a specific role in anion binding. Thus, although the groups Asp-85 and Asp-212 have clearly been shown to participate directly in the complex counterion and Cl^- binding, the necessary additional positive group has still to be identified.

This work was supported by grant from Országos Tudományos Kutatási Alap (OTKA). T017017

REFERENCES

Aton, B., A. G. Doukas, R. H. Callender, B. Becher, and T. G. Ebrey. 1977. Resonance Raman studies of the purple membrane. *Biochemistry.* 16: 2995–2998.

Bellamy, L. J. 1980. The Infrared Spectra of Complex Molecules. Chapman and Hall, London.

Braiman, M. S., A. K. Dioumaev, and J. R. Lewis. 1996. A large photolysis-induced pK_a increase of the chromophore counterion in bacteriorhodopsin: implications for ion transport mechanisms of retinal proteins. *Biophys. J.* 70:939–947.

Braiman, M. S., T. J. Walter, and D. Briercheck. 1994. Infrared spectroscopic detection of light-induced change in chloride-arginine interaction in halorhodopsin. *Biochemistry.* 33:1629–1635.

Le Coutre, J., M. Rüdiger, D. Oesterhelt, and K. Gerwert. 1995. FTIR investigation of the blue to acid-purple transition of Bacteriorhodopsin by use of induced halide binding. *J. Mol. Struct.* 349:165–168. de Groot, H. J. M., S. O. Smith, J. Courtin, E. van den Berg, C. Winkel, J. Lugtenburg, R. G. Griffin, and J. Herzfeld. 1990. Solid-state ^{13}C and ^{15}N NMR study of the low pH forms of bacteriorhodopsin. *Biochemistry.* 29:6873–6883.

Dér, A., R. Tóth-Boconádi, and L. Keszthelyi. 1989. Bacteriorhodopsin as a possible chloride pump. *FEBS Lett.* 259:24–26.

Dér, A., S. Száraz, R. Tóth-Boconádi, Zs. Tokaji, L. Keszthelyi, and W. Stoeckenius. 1991. Alternative translocation of protons and halide ions by bacteriorhodopsin. *Proc. Natl. Acad. Sci. USA.* 88:4751–4755.

Dioumaev, A. K., and M. S. Braiman. 1995. Modelling vibrational spectra of amino acid side chains in proteins: the carbonyl stretch frequency of buried carboxylic residues. *J. Am. Chem. Soc.* 117:10572–10574.

Fischer, U., and D. Oesterhelt. 1979. Chromophore equilibria in bacteriorhodopsin. *Biophys. J.* 28:211–230.

Gertner, B. J., and J. Hynes. 1996. Molecular dynamics simulation of hydrochloric ionization at the surface of stratospheric ice. *Science.* 271:1563–1566.

Gerwert, K., U. M. Ganter, F. Siebert, and B. Hess. 1987. Only water exposed carboxyl-groups are protonated during the transition to the cation-free blue bacteriorhodopsin. *FEBS Lett.* 213:39–44.

Kalaidzidis, I. V., and A. D. Kaulen. 1997. Cl^- dependent photovoltage responses of bacteriorhodopsin: comparison of the D85T and D85S mutants and wild-type acid purple form. *FEBS Lett.* 418:239–242.

Keszthelyi, L., S. Száraz, A. Dér, and W. Stoeckenius. 1990. Bacteriorhodopsin and halorhodopsin: multiple ion pumps. *Biochim. Biophys. Acta.* 1018:260–262.

Lányi, J. K. 1990. Halorhodopsin: a light-driven electrogenic chloride transport system. *Physiol. Rev.* 70:319–330.

Lányi, J. K., L. Zimányi, K. Nakanishi, F. Derguini, M. Okabe, and B. Honig. 1988. Chromophore/protein and chromophore/anion interactions in halorhodopsin. *Biophys. J.* 53:185–191.

Marrero, H., and K. J. Rothschild. 1987. Bacteriorhodopsin's M_{412} and BR_{605} protein conformations are similar. *FEBS Lett.* 223:289–293.

Marti, T., S. J. Rösselet, H. Otto, M. P. Heyn, and H. G. Khorana. 1991. The retinylidene Schiff-base counterion in bacteriorhodopsin. *J. Biol. Chem.* 288:18674–18683.

Masuda, S., M. Nara, M. Tasumi, M. A. El-Sayed, and J. K. Lányi. 1995. Fourier transform infrared studies of the effect of Ca^{2+} binding on the states of aspartic acid side chains in bacteriorhodopsin. *J. Phys. Chem.* 99:7776–7781.

Metz, G., F. Siebert, and M. Engelhardt. 1992. Asp-85 is the only internal aspartic acid that gets protonated in the M intermediate and the purple-to-blue transition of bacteriorhodopsin. *FEBS Lett.* 303:237–241.

Mitrovich, Q. M., G. V. Kenneth, and M. S. Braiman. 1995. Differences between the photocycles of halorhodopsin and the acid purple form of bacteriorhodopsin analyzed with millisecond time-resolved FTIR spectroscopy. *Biophys. Chem.* 56:121–127.

Moltke, S., and M. P. Heyn. 1995. Photovoltage kinetics of the acid-blue and acid-purple forms of bacteriorhodopsin: evidence for no net charge transfer. *Biophys. J.* 69: 2066–2073.

Mowery, P. C., R. H. Lozier, Q. Chae, Y. W. Tseng, M. Taylor, and W. Stoeckenius. 1979. Effect of acid pH on the absorption spectra and photoreactions of bacteriorhodopsin. *Biochemistry.* 18:4100–4107.

Oesterhelt, D., and W. Stoeckenius. 1971. Rhodopsin-like protein from the purple membrane of *Halobacterium halobium*. *Nature New Biol.* 233: 149–152.

Oesterhelt, D., and W. Stoeckenius. 1974. Isolation of the cell membrane of *Halobacterium halobium* and its fractionation into red and purple membrane. *Methods Enzymol.* 31:667–668.

Oesterhelt, D., and J. Tittor. 1989. Two pumps, one principle: light-driven ion transport in halobacteria. *Trends Biol. Sci.*14:57–61.

Rath, P., M. P. Krebs, Y. He, H. G. Khorana, and K. J. Rothschild. 1993. Fourier transform Raman spectroscopy of the bacteriorhodopsin mutant Tyr-185→Phe: formation of a stable O-like species during light adaptation and detection of its transient N-like photoproduct. *Biochemistry.* 32:2272–2281.

Renthal, R., K. Shuler and R. Regalado. 1990. Control of bacteriorhodopsin color by chloride at low pH: significance for the proton pump mechanism. *Biochim. Biophys. Acta.* 1016:378–384.

Rothschild, K. J. 1992. FTIR difference spectroscopy of bacteriorhodopsin: toward a molecular model. *J. Bioenerg. Biomemb.* 24:147–167.

Sasaki, J., L. S. Brown, Y.-S. Chon, H. Kandori, A. Maeda, R. Needleman, and J. K. Lányi. 1995. Conversion of bacteriorhodopsin into a chloride ion pump. *Science.* 269:73–75.

Sawatzki, J., R. Fischer, H. Scheer, and F. Siebert. 1990. Fourier-transform Raman spectroscopy applied to photobiological systems. *Proc. Natl. Acad. Sci. USA.* 87:5903–5906.

Smith, O. S., and R. A. Mathies. 1985. Resonance Raman spectra of the acidified and deionized forms of bacteriorhodopsin. *Biophys. J.* 47: 251–254.

Stoeckenius, W., R. H. Lozier, and R. A. Bogomolni. 1979. Bacteriorhodopsin and the purple membrane of halobacteria. *Biochim. Biophys. Acta.* 505:215–27.

Száraz, S., D. Oesterhelt, and P. Ormos. 1994. pH-induced structural changes in bacteriorhodopsin studied by Fourier transform infrared spectroscopy. *Biophys. J.* 67:1706–1712.

Váró, G., and J. K. Lányi. 1989. Photoreactions of bacteriorhodopsin at acid pH. *Biophys. J.* 56:1143–1151.

Biophysical Journal Volume 81 December 2001 3577–3589

Structural Changes in Bacteriorhodopsin during the Photocycle Measured by Time-Resolved Polarized Fourier Transform Infrared Spectroscopy

Lóránd Kelemen and Pál Ormos
Institute of Biophysics, Biological Research Centre of the Hungarian Academy of Sciences, Szeged H-6701, Hungary

ABSTRACT The structural changes in bacteriorhodopsin during the photocycle are investigated. Time resolved polarized infrared spectroscopy in combination with photoselection is used to determine the orientation and motion of certain structural units of the molecule: Asp-85, Asp-96, Asp-115, the Schiff base, and several amide I vibrations. The results are compared with recently published x-ray diffraction data with atomic resolution about conformational motions during the photocycle. The orientation of the measured vibrations are also calculated from the structure data, and based on the comparison of the values from the two techniques new information is obtained: several amide I bands in the infrared spectrum are assigned, and we can also identify the position of the proton in the protonated Asp residues.

INTRODUCTION

The protein pigment complex bacteriorhodopsin (bR) is found in high protein content regions of the cell membrane of *Halobacterium salinarum*, called the purple membranes. The chromophore is retinal connected to the Lys-216 residue of the protein backbone through a protonated Schiff base. bR is a light energy transducer upon light absorption it pumps protons across the cell membrane. After the absorption of a photon by retinal a sequence of reactions takes place: the photocycle. The photocycle runs through several intermediates (designated K, L, M, N, O) that are well distinguished by their visible absorption spectra.

Conformational changes of the protein are generally regarded crucial for the proton pumping function of bR. The correlated motion of both the chromophore and the protein moiety form the basis of the active pumping, consequently, the characterization of the molecular motions is the key to understanding the energy conversion process. By correlating structural and functional data,several structural markers have been found to characterize conformational changes that seem to be crucial for pumping. However, an exact identification of key conformational transitions in the photocycle could not be achieved. A number of methods have been used to investigate the protein structural changes that accompany the photocycle. Recently several results have been published in which the structure of bR was determined with atomic resolution, including the structures of several intermediate states of the pumping cycle. The first markers of the crucial structural changes have been determined and characterized in fairly great detail by Fourier transform infrared (FTIR) spectroscopy. A next step in the understanding is the identification of these markers with the recently determined molecular structures.

To characterize the orientation of a structural element in bR two angles are needed. A practical procedure is offered in FTIR spectroscopy, if the sample is a hydrated film of purple membranes oriented on an infrared (IR) window surface. On such a sample the option is to measure the angle of the element's IR dipole moment relative to the purple membrane normal in one experiment and then the angle between the projection of the element's IR dipole moment and that of the retinal's optical transition moment onto the purple membrane plane in a separate one. The first measurement does not need polarized actinic light but needs polarized IR measuring beam and measurement of the sample in two different sample positions relative to the IR beam.

We note here that the retinal position has previously been determined by polarized spectroscopy both in the visible (Barabás et al., 1983; Heyn and Otto, 1992) and in the IR (Earnest et al., 1986). The visible experiments resulted in an angle of ~67° between the retinal transition dipole and the membrabe normal. This is in agreement with the IR experiment in which the direction of the IR dipole moment of the retinal's delocalized C=C stretch, which is expected to be parallel to the axis of the polyene chain, also makes an angle of 64 to 71° with the normal of the PM plane in the bR state. The authors determined also the orientation of the dipole of the C=O stretch in the protonated Asp-85 side chain in the M state relative to the PM normal. The angle between the two directions turned out to be 43 ± 4°. This value is contradicted by Hatanaka et al. (1997) and Nabedryk and Breton (1986) in both latter papers this angle was found to be ~35° (36° and 35 ± 5°, respectively). Nabedryk and Breton (1986) additionally made estimations about the tilt of the protein backbone between the bR and the M states and concluded that the overall orientational change of the α-helices is ~2°. However, local conformational changes cannot be and were not excluded.

Received for publication 3 May 2001 and in final form 23 August 2001.
Address reprint requests to Institute of Biophysics, Biological Research Centre of the Hungarian Academy of Sciences, Szeged H-6701, Hungary. Tel.: 36-62-433465; Fax: 36-62-433133; E-mail: pali@everx.szbk.u-szeged.hu.

0006-3495/01/12/3577/13 $2.00

The angle Θ between the projection of a structural element's IR dipole moment and that of the retinal's optical transition moment onto the PM plane can be determined by photoselective excitation and polarized IR measurement of an oriented bR sample (Fahmy et al., 1989, 1991; using slightly different nomenclature). In the first work the authors showed that in the ground state the direction of the retinal's C=C IR dipole moment makes an angle to the PM normal identical to that found for the optical transition moment and additionally proved that the angle Θ for this dipole is also zero. This simply means that the direction of the IR and the optical dipole moments coincide in the ground state. The Schiff base as the primary proton donor plays a key role in the proton transfer function of the protein. Its orientation therefore is crucial for the understanding of the events inside bR. Fahmy et al. (1989) determined without detailed calculations that the dipole of the Schiff-base's C=N stretch is perpendicular to the PM normal and that its angle Θ is approximately zero in the ground state. Later the same authors determined the orientation of several amino acid side chains also relative to both the PM normal and the retinal's optical transition (Fahmy et al., 1991). In the L state both the Asp-96 and Asp-115 groups give a positive band in the COOH region of the IR spectrum. Detailed analysis of these difference bands led to the conclusion that these two groups do turn between the bR and L states. The movement of the dipole moments is larger in the direction of the PM normal (~25°) than parallel to its plane (4–11°). This result is important because in the L state the primary proton movement from the Schiff base to Asp-85 has not yet occurred, but apparently rearrangement of important side chains has already started at some level. The direction of Asp-85 in the M state was characterized in greater detail by Breton and Nabedryk (1989) who measured the angle Θ of its C=O stretch to be 45°. This value and the previously found 43° (Earnest et al., 1986) (35° by Hatanaka et al., 1997) gives an approximation to the direction of the dipole of this amino acid side chain in the M state.

The aim of the presented work was to obtain new structural data from FTIR measurements and compare these with recent x-ray diffraction information. We performed experiments to determine values of Θ for bands of the IR difference spectra of the M or N states. For this we carried out time-resolved low-temperature polarized FTIR measurements combined with photoselection on wild-type bR. Our first goal was to estimate a direction relative to the retinal by using the angle Θ for several structural elements of bR to which an IR difference band was previously assigned. Next, we tried to assign amide I bands to parts of the bR backbone by comparison of the angle Θ measured with values calculated using recently published x-ray diffraction structures. By this procedure the structural information obtained by the different experimental techniques is expected to be unified, and an approach is made toward a coherent picture of the structural changes during function.

METHODS AND MATERIALS

Purple membranes of wild-type bR used for the photoselection measurements were prepared from strain S9 of *Halobacterium salinarum* (Oesterhelt and Stoeckenius, 1974). For the dried-rehydrated film a bR suspension of OD = 8 was prepared in 100 μM Trizma solution. Fifty microliters of this suspension was spread over an 8-mm diameter area on a 2-mm-thick CaF_2 window. This drop of suspension was dried under a gentle N_2 stream blowing downwards from above the center of the droplet, perpendicularly to the plane of the CaF_2 window. This way the inner 5 mm of the sample dried with even optical density suitable for homogeneous excitation and IR measurements. The CaF_2 window was placed into a temperature-controlled sample holder with the bR film facing inside. Approximately 3 μl of water was additionally dropped into the sample holder to rehydrate the bR film. Another 2-mm-thick CaF_2 window was used to hermetically seal the sample holder. The IR absorption of the dry sample was 0.65 in the amide I region at 1657 cm^{-1}, whereas that of the rehydrated sample was 0.9. The 3500-cm^{-1} water absorption band was used to check the process of rehydration. After 2 days this band was ~1.4 times larger than the absorption at 1657 cm^{-1}. The sample was masked by a 4-mm diameter aperture at its central region to make sure that the IR monitoring light and the exciting light illuminate identical part of the sample. The sample was kept at −8°C (265 K) throughout the entire measurement, and at this temperature 50 s after the start of the photocycle only 0.5% of the original difference signal remained, i.e., the total recovery of the bR state took ~1 min.

To facilitate photoselection the sample had to consist of aligned PM fragments. This property of our sample was checked by the method introduced in Rothschild and Clark (1979): using horizontally polarized IR beam we measured the IR absorption of the sample with the bR film's plane perpendicular to the IR beam (A_0) and when it was rotated 45° around the vertical axis (A_{45}). We calculated a dichroic difference spectrum from the two resulted absorption spectra (A_0–A_{45}). This showed an intense negative peak at 1667 cm^{-1} (amide I), one at 3250 cm^{-1} (amide A), and a positive one at 1548 cm^{-1} (amide II) (Fig. 1). The dichroic difference spectra were very similar to the one published on sample of aligned PM by Rothschild and Clark (1979).

The flash from a frequency doubled YAG laser (SURELITE I, Continuum, Santa Clara, CA) (λ = 532 nm, duration = 5 ns) started the photocycle. To not excite any intermediate in the repetitive experiments the sample was flashed in every 60 s. For the photoselection the exciting light had to be linearly polarized. Although the light emitted by the laser is already polarized, we applied a VIS polarizer to improve the polarization characteristics of the exciting light. The original beam diameter of the laser (~4 mm) was expanded to ~1 cm at the sample to ensure that only a homogeneous intensity region of the laser spot hits the sample and also to reduce the laser intensity. The laser intensity was chosen so that the amplitude of the calculated difference spectra was only 11% of that measured at saturation. The actinic laser light hit the sample with an angle of ~8° relative to the sample normal and to the direction of the IR beam.

The FTIR measurements were carried out on a Bruker IFS66 instrument (Bruker Optik GmbH, Ettlingen, Germany) capable of measuring with 85-ms time resolution in rapid scan mode. The IR bandwidth was reduced to 800 to 1970 cm^{-1} partly by the absorption of the CaF_2 window and partly by a low wavelength pass optical filter (L.O.T.–Oriel GmbH, Langenberg, Germany) that also blocked the detector from the YAG laser light. The spectral resolution of the measurement was 4 cm^{-1}, this parameter together with the fastest mirror scanning allowed the above time resolution. The zero filling factor was 4, this resulted data points in every 0.63 cm^{-1}. The measuring IR light was focused perpendicularly at the sample onto a spot of ~4 mm diameter. The small axial difference between the actinic and the measuring light beam directions did not introduce noticeable error to the measurement.

The IR polarizer for the linear dichroic measurement was a golden wire grid polarizer on KRS-5 glass (International Crystal Labs, Garfield, NJ), and it was placed between the sample holder and the detector. It was rotated to parallel and perpendicular positions relative

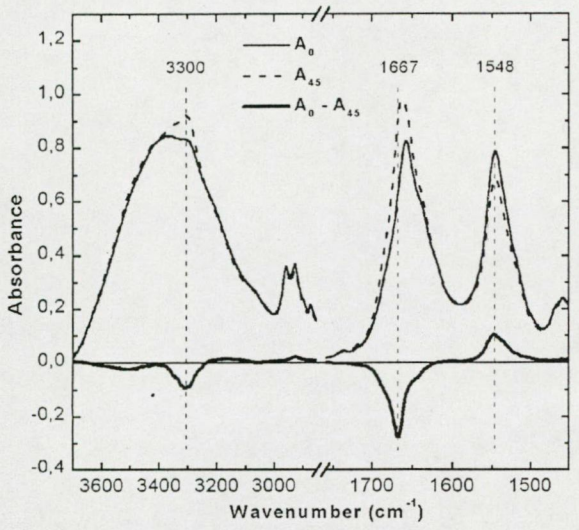

FIGURE 1 Absorption and dichroic spectra of rehydrated dried bR film measured in horizontally polarized IR light. The plane of the film is perpendicular to the optical axis of the IR beam (A_0) (*thin line*). The plane of the film is tilted 45° around the vertical axis, i.e., the normal of the film makes 45° with the optical axis of the IR beam (A_{45}) (*dashed line*). Dichroic spectrum (A_0–A_{45}) (*thick line*).

to the actinic laser light polarization by a small program embedded in the measuring OPUS software (Bruker Optik GmbH). One-hundred measurements with parallel and 100 measurements with perpendicular orientation were repeated 25 times, resulting in 2500 averages with both polarizer positions.

The raw results of the measurements were a series of single beam spectra, i.e., intensity spectra. The synchronization of the start of the measurement and the actinic laser flash was done such that the very first spectrum was measured just before the laser flash and stored as background ($SB(\lambda, t = 0)$), the others were measured after the flash ($SB(\lambda, t)$) in a predetermined sequence. Each spectrum in the time-resolved series needed a full scan of the interferometer, represented by its start-of-scan time and end-of-scan time. The time point corresponding to each spectrum was the average of these two characteristic times. The data acquisition was set up such that the spectra were averaged quasi-logarithmically to increase the S/N ratio: the first eight spectra were the result of single scans, every spectrum of the second eight was the average of two consecutive scans, every spectrum of the third eight was average of four consecutive scans, and so on. This way the final series contained 50 spectra spanning the 60-s measurement. The best time resolution was 85 ms at the beginning of the measurement, the worst was ~5.4 s at the end.

Data processing

Difference spectra were calculated from the measured single beam spectra as follows:

$$D(\lambda, t) = -\log \frac{SB(\lambda, t)}{SB(\lambda, t = 0)}$$

in which $D(\lambda, t)$ is the difference spectrum series consisting of 50 spectra, $SB(\lambda, t)$, and $SB(\lambda, t = 0)$ as described above. This calculation was performed on the data of both parallel and perpendicular polarization directions relative to the polarization of the actinic light resulting $D_{\parallel}$ and $D_{\perp}$, respectively. The difference spectra showed maximal amplitude at the first time-slice and gradually decayed to zero by the end of the 60-s-long measurement. We did not apply any noise reduction on the difference spectra before the additional calculations.

In previous papers (Breton and Nabedryk, 1989; Fahmy et al., 1991) the angle Θ was calculated using the amplitude of the IR bands taken directly from the difference spectra. This method cannot be applied for overlapping bands. To overcome this problem and to make this method usable for amide I difference bands, we first fitted sums of Gaussians to the difference spectra and then we used the time-dependent amplitudes of these Gaussian bands to determine Θ. We used global algorithm to fit the $D_{\parallel}$ and $D_{\perp}$ spectrum series together as one single series, i.e., the Gaussian band positions and half-widths constituted an identical set for all of the 2 × 50 spectra, and only the amplitude of each Gaussian band was allowed to change from spectrum to spectrum. The resulted series of Gaussian amplitudes were $A_{\parallel}(t)$ and $A_{\perp}(t)$ for the two orientation directions consisting of 50-50 values each. The algorithm also added either a linear baseline (COOH region) or a constant baseline (amide I region) to the Gaussians. Because we dealt only with the changes of COOH groups and the protein backbone we performed the fitting only in limited regions: in regions 1712 to 1820 cm^{-1} and 1613 to 1704 cm^{-1}.

In addition, the time-dependent Gaussian amplitudes $A_{\parallel}(t)$ and $A_{\perp}(t)$ were globally fitted with sums of three exponentials, which means that all of the Gaussian amplitudes had the same time constants (τ_1, τ_2, and τ_3) but different exponential amplitudes. Three exponentials were sufficient for the fitting because applying four exponentials always resulted in degenerated results.

The calculation of the angle Θ was carried out using the Gaussian amplitudes (Breton and Nabedryk, 1989):

$$\Theta(t) = \arccos\left(\left(\frac{A_{\parallel}(t) - A_{\perp}(t)}{A_{\parallel}(t) + A_{\perp}(t)} + 0.5\right)^{1/2}\right) \qquad (1)$$

This angle could be calculated for every IR band that can be fitted to a Gaussian. Because every band originates from the vibration of a dipole, this angle can be attributed to vibration modes and hence to structural elements. This way we determined the angle between the projection of the retinal and the projection of the particular structural element on the plane of the PM.

RESULTS AND DISCUSSION

We made polarized photoselection measurement on wild-type bR at T = −8°C (265 K) on rehydrated dried sample. The resulting $D_{\parallel}$ and $D_{\perp}$ difference spectra show very good signal-to-noise ratio: the noise ~1780 cm^{-1} where there is no difference signal was ~10^{-6} OD, and the maximal signal at 1526 cm^{-1} was 2 × 10^{-3} OD (Fig. 2). However, ~1640 cm^{-1} where the water and the amide I absorption is high, there can be higher noise as well, but fortunately the signal is also large in that region. This S/N was sufficient for meaningful Gaussian fitting.

In Fahmy et al. (1991) the angle Θ is calculated using a factor c that enlarges dichroic difference $A_{\parallel}$–$A_{\perp}$ to the value that would be found for complete photoreaction:

$$\tan^2 \Theta = \left(\frac{A_{\parallel}(t) + A_{\perp}(t) - c \times (A_{\parallel}(t) - A_{\perp}(t))}{A_{\parallel}(t) + A_{\perp}(t) + c \times (A_{\parallel}(t) - A_{\perp}(t))}\right) \qquad (2)$$

This correction was considered necessary for reasons such as light scattering in the sample and that in a realistic photoselection measurement the excitation may be higher than the optimal low intensity limit and the saturation effect

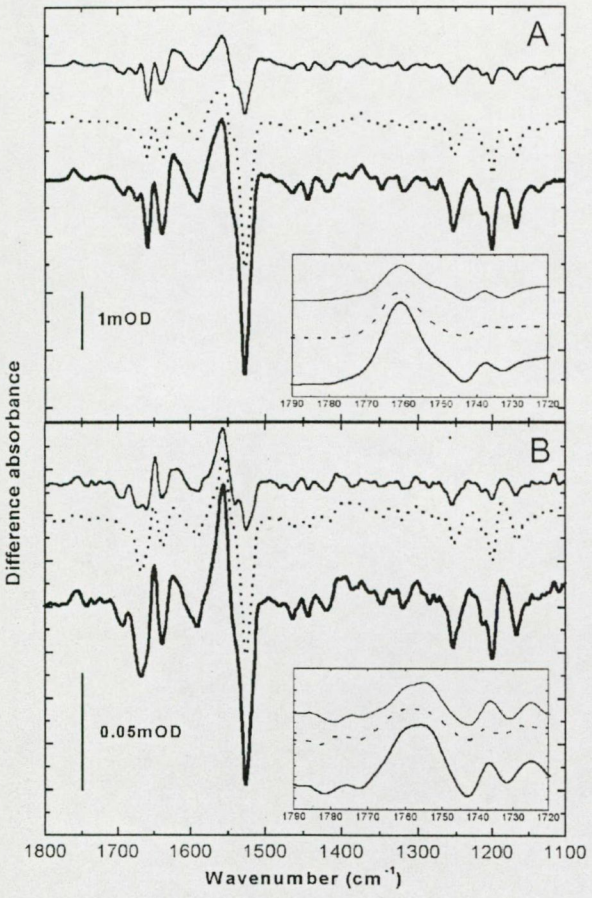

FIGURE 2 Difference spectra of rapid scan photoselection measurements (polarized actinic and measuring light) performed on rehydrated bR film ($T = -8°C$) 78 ms (*a*) and 30 s (*b*) after the photoexcitation. The polarization of the actinic and the measuring light were either parallel (D_{II}; *dashed line*) or perpendicular ($D_{\perp}$; *thin line*) to each other. The sum of the two orientations is represented by the (*thick line*) ($D_{II} + D_{\perp}$). Inserts, The expanded COOH region.

decreases the anisotropy. The authors showed that for the 1527 cm^{-1} C=C retinal band (Fahmy et al., 1989) Θ is zero, and they used its dichroic ratio to calculate the value of c, which was found to be 7 to 10. Using the same calculation we determined c for our measurement based on the intensity of the 1527 cm^{-1} band, and it turned out to be 2. This means that in our case the simpler Eq. 1 is valid, no additional correction is necessary.

COOH region

To determine the Gaussian amplitudes of the IR bands in the carboxyl vibration region we fitted the spectrum series with sums of Gaussians plus a linear baseline from 1712 cm^{-1} to 1820 cm^{-1} (Fig. 3, *a* and *b*). The linear baseline was needed because of the presence of the water continuum band in this region (Rammelsberg et al., 1998). The intensities of the COOH bands are small as compared with the rest of the spectrum, and at the later time slices of the spectra series the fit was uncertain. For this reason the region was fitted only for spectra taken in the 0 to 20-s interval.

The obtained bands well correspond to the band positions observed in the M and N intermediates: the 1761 cm^{-1} and 1738 cm^{-1} positive bands are typical for the M, whereas the 1756 cm^{-1} positive and 1743 cm^{-1} negative bands are typical for the N state (Ormos et al., 1992; Sasaki et al., 1994; Yamazaki et al., 1998) (Table 1). We also obtained another positive band at 1725 cm^{-1} with intensity similar to that of the 1738 cm^{-1} band. It can also be observed in the M spectrum of the polarized measurement in Nabedryk and Breton (1986). The origin of this band is not clear at the moment, but one possibility is the special alignment characteristics of the sample. However, this band was too wide and its time-dependent intensity was too noisy, giving unreliable Θ value.

The time-dependent Gaussian amplitudes of the COOH bands (both A_{II} and $A_{\perp}$) could be fitted to a sum of three exponentials (Fig. 3, *c* and *d*). The obtained τ values were: 0.33 s, 2.53 s, and 11.66 s. Table 1 depicts the exponential amplitudes for the COOH bands. The fact that the exponential fitting gave three macroscopic rate constants shows that there are three intermediate forms involved (Nagle, 1991). Because the very first difference spectrum at $t = 78$ ms is that of an almost pure M, only the presence of forms after the M intermediate is possible. In addition, from the kinetic analysis of Váró and Lányi (1991), it follows that the early M is not present anymore at this time. We know that at low temperatures the O form is not present either (Ludmann et al., 1998; Váró and Lányi, 1991), therefore the measured difference spectra are mixtures of the M and N forms. In this work we do not attempt to perform a detailed kinetic analysis, but assume that some of the three exponential components describe M→N transition and some of them N→bR decay. This is supported by that in the case of the negative 1743 cm^{-1} and the positive 1756 cm^{-1} bands, both typical for the N state, the sign of the first exponential amplitude (a_1) is different form the last two (a_2, a_3), meaning that the a_1 represents an M→N transition, whereas the a_2 and a_3 belong to decays. The exponential amplitudes of the 1761 cm^{-1} band all have positive sign, showing its decay throughout the whole process. The opposite sign and large absolute value of a_1 relative to a_2 and a_3 in the case of the 1756 cm^{-1} band indicate that this band is still building up during at least the first 500 ms of the measurement. Because this band is characteristic to the N state, we can conclude that by ~1 s large population of the bR transformed from M to N. The a_3 amplitude of this band and that of the 1743 cm^{-1} band are the largest in both cases, which shows that this exponential amplitude most likely represents the N→bR decay.

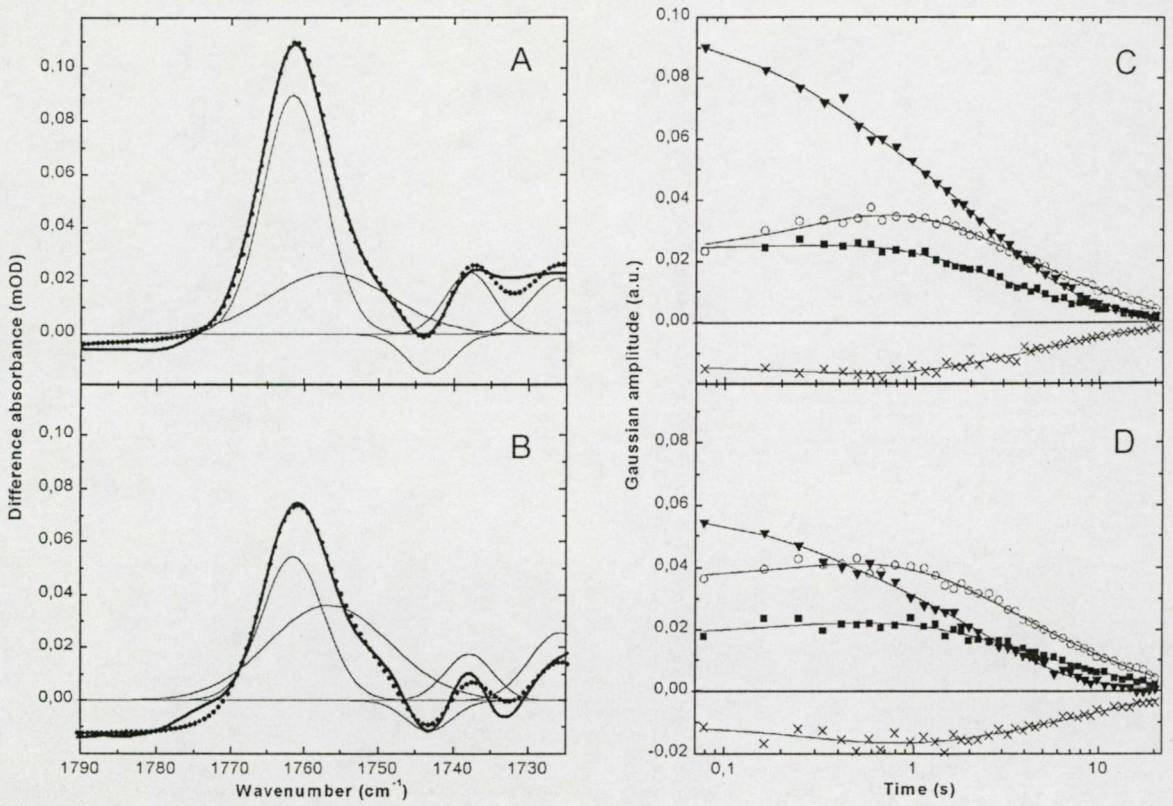

FIGURE 3 Gaussian fit to the 1712 cm^{-1} to 1820 cm^{-1} region of the photoselection difference spectra measured on rehydrated bR film ($T = -8°C$). Figures on the left (parallel polarization (*a*) and perpendicular polarization (*b*)) show the original difference spectra 78 ms after photoexcitation (*thick line*), the fitted curves to these early spectra (*dotted line*), and the individual Gaussian components (*thin line*). Figures on the right (parallel polarization (*c*) and perpendicular polarization (*d*)) show the time evolution of the Gaussian amplitudes of the 1738 cm^{-1} (■), the 1743 cm^{-1} (×), the 1756 cm^{-1} (○), and the 1761 cm^{-1} (▼) bands together with the exponential fit to these time dependent amplitudes (*thin line*).

In Table 1 there are two Θ values indicated for each band. The first one always corresponds to Θ at $t = 78$ ms, the last one to Θ at $t = 20$ s after the start of the photocycle, except the 1761 cm^{-1} band, where the last one corresponds to 8 s. This is because the Gaussian amplitudes $A_{\parallel}$ and $A_{\perp}$ of the 1761 cm^{-1} band become too small after 8 s so the ratio in Eq. 1 gives large noise.

The Θ angle values calculated from the Gaussian fitting change slightly with time (Fig. 4). This may come either from uncertainties of the fitting, because of the relatively small signal in this region, or from the fact that the orientation of the COOH groups change in time indeed. The first explanation is more likely because such a continuous change in side-chain orientation would result in change of

TABLE 1 Result of the Gaussian fit to the difference spectra in the COOH region

Band position	1761 cm^{-1}	1756 cm^{-1}	1743 cm^{-1}	1738 cm^{-1}
Sign of the band	Positive	Positive	Negative	Positive
Θ Value	30–25°	55–47°	40–55°	40–53°
Exponential amplitudes for $A_{\parallel}$ spectra ($a_{i,\parallel}$), $i = 1, 2, 3$	$a_1 = 0.279$ $a_2 = 0.582$ $a_3 = 0.116$	$a_1 = -0.226$ $a_2 = 0.208$ $a_3 = 0.235$	$a_1 = 0.062$ $a_2 = -0.088$ $a_3 = -0.111$	$a_1 = -0.069$ $a_2 = 0.213$ $a_3 = 0.094$
Exponential amplitudes for $A_{\perp}$ spectra ($a_{i,\perp}$), $i = 1, 2, 3$	$a_1 = 0.161$ $a_2 = 0.385$ $a_3 = 0.044$	$a_1 = -0.142$ $a_2 = 0.232$ $a_3 = 0.264$	$a_1 = 0.091$ $a_2 = -0.037$ $a_3 = -0.158$	$a_1 = -0.091$ $a_2 = 0.128$ $a_3 = 0.144$
Assigned to	Asp-85 in M	Asp-85 in N	Asp-96 in N	Asp-115 in M, N

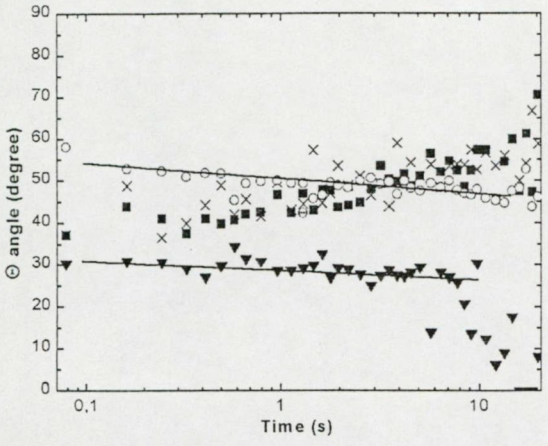

FIGURE 4 The time dependence of the angle Θ between the projection of the retinal's IR dipole moment to the membrane plane and that of the IR dipole moments of COOH groups responsible for the individual bR difference bands: 1738 cm^{-1} (■), 1743 cm^{-1} (×), 1756 cm^{-1} (○), and 1761 cm^{-1} (▼). The continuous lines are inserted only to guide the eye.

the environment of the group, and this latter would give rise to a continuous frequency shift, too. This kind of band shift was not observed in our data. The time independence of the angle Θ generalizes earlier results of Czégé et al. (1982), who found that the anisotropy factor of ultraviolet chromophores, i.e., tryptophan does not change while they are in a perturbed state. These results indicate that the protein parts observed have constant orientation during the lifetime of a particular intermediate, i.e., all conformational changes are synchronized to the well-known transitions in the photocycle.

We know from the literature that both the 1761 cm^{-1} and the 1756 cm^{-1} bands originate from the C=O stretching vibration of the protonated Asp-85 group: the first band is present in the M state, the latter one is in the N state (Kandori, 1998; Sasaki et al., 1994; Ormos et al., 1992). The difference in the frequency is due to the different environment of the group in the two intermediates. The nature of this environmental change between M and N has not been yet clarified, in other words it has not been answered whether the environmental change is connected to the movement of this group (when the direction of the C=O dipole does change), or it happens without any movement (for example a formation of a new H bond to the Asp-85 and the orientation of the dipole remains the same) (Heberle, 2000; Sasaki et al., 1994). There is only one hint for the position of the Asp-85 in the literature: in Kandori (1998) it is stated that there is no significant change in its position between M and N. We note that this statement is based only on the measurement of the angle between the dipole moment and the normal of the PM plane, and therefore it is necessarily an underassumption.

Our measurement is, however, a direct proof that this group does change its orientation during the M→N transition. For the 1761 cm^{-1} band that is the frequency of the Asp-85 in the M state we measured $\Theta < 30°$ and for the 1756 cm^{-1}, which is its frequency in the N state we obtained $45 < \Theta < 55°$ during the whole process. This means that the projection of the vibration mode of the group's C=O stretching onto the membrane plane clearly changes its orientation during M→N by ~20°. Because this value refers only to the projection of the movement, the absolute rotation can be even larger.

The directions of the CO bonds of the Asp-85, Asp-96, and Asp-115 carboxyl groups were calculated using recent x-ray structural models of the bR, M, and M_N intermediates. The bond directions can also be determined from the FTIR difference spectra. In control normal mode calculation on formic acid as a model for the protonated carboxyl group we determined that the direction of the vibrational dipole moment of the C=O stretching mode deviates less than 4° from the direction of the C=O bond, which is less than the error of our measurement. Based on these two calculations a comparison was made between the Θ angle values measured by FTIR (Table 1) and the directions of the CO bonds obtained from the x-ray structures (Table 2). The two angle values in each row of Table 2 refer to the directions of the two CO bonds in the carboxyl groups.

In the case of Asp-85 for both chosen M-state structures the calculated CO angles (48 and 51°) of the first O atom

TABLE 2 Directions of CO bonds of carboxyl groups in ground state (bR) and in M or M_N state calculated from x-ray structures of wild-type (WT) and mutant bacteriorhodopsin

		WT bR	WT bR	WT M	E204Q bR	E204Q M	D96N M_N
Asp-85 (M)	1st O			48°		51°	
	2nd O			86.5°		82°	
Asp-85 (N)	1st O						82.5°
	2nd O						68°
Asp-96	1st O	58°	65°		64°		
	2nd O	36°	38.5°		36.5°		
Asp-115	1st O			45°		38.5°	43.5°
	2nd O			84°		84°	64.5°
References		Belrhali et al., 1999	Sass et al., 2000	Sass et al., 2000	Luecke et al., 2000	Luecke et al., 2000	Luecke et al., 1999

agree fairly well with the Θ angle measured for the protonated group in the M state (1761 cm^{-1} band, 25–30°). (The agreement is even better if we consider that in the structure of Sass et al. (2000) the measured structure is assumed to be a mixture of M and N, and the Θ value for the 1756 cm^{-1} N band is 47–55°.) This oxygen is the one pointing away from the retinal, which indicates that this forms the C═O bond, and the other O atom pointing toward the Schiff base participates in the C—O bond, bearing the accepted H. This supports the general notion that the O atom, which in the ground state is H bonded to the water molecule localized between the Schiff base and Asp-85 gets protonated in M.

Note that by identifying the C═O bond, this method is capable of determining which oxygen is protonated in a carboxyl group. The same procedure can be applied to the other aspartic residues, too.

The negative 1743 cm^{-1} band, which shows the deprotonation of the Asp-96 group (Gerwert et al., 1990), is still growing at the beginning of the measurement and has negative a_1 and positive a_2 and a_3 exponential amplitudes, which corresponds to the fact that this band is present in the N state. From this negative band it follows that the projection of the IR transition dipole of the C═O stretch of the Asp-96 group in the ground state makes an 47 ± 7° angle with that of the retinal (Table 1). The angles calculated for the second CO bond of Asp-96 are reasonably close to this range for all three x-ray models (Table 2). This agreement is better than for Asp-85 and indicates that the unprotonated O atom of Asp-96 in the ground state is pointing to the center of the molecule, and the one pointing to the cytoplasmic side will subsequently donate its proton to the Schiff base.

The 1738 cm^{-1} positive band is the result of the environmental change of the protonated Asp-115 residue that evolves during the M state and remains present throughout the N state (Sasaki et al., 1994). Its measured Θ value matches the first CO bond's angle value for all three x-ray structures. This C═O bond in the ground state consequently points toward the extracellular surface.

Amide I region

Twelve bands were needed for the fitting of the amide I region of the difference spectra between 1613 cm^{-1} and 1704 cm^{-1} with sums of Gaussians and a constant baseline. There were bands that resulted in negligible Gaussian amplitude either in the A_{II} or in the $A_{\perp}$ spectrum, but which were necessary to fit the two types of spectra together. Whereas these bands could not be used for Θ angle calculation, the rest of the bands that are characteristic for the difference spectrum of the M or the N state (Ormos, 1991; Ormos et al., 1992; Rothschild et al., 1993; Yamazaki et al., 1998) could be fitted precisely and gave reliable Gaussian amplitudes and Θ values. The maximal residuum of the fit was smaller than 5% of the signal.

The characteristic main bands were fitted to the following positions: 1624 cm^{-1} ⊕, 1639 cm^{-1} ⊖, 1652 cm^{-1} ⊕, 1657 cm^{-1} ⊖, 1667 cm^{-1} ⊖, 1674 cm^{-1} ⊖, 1692 cm^{-1} ⊖, and 1699 cm^{-1} ⊖ (Fig. 5, *a* and *b*) (⊕, positive band: ⊖, negative band). The first two bands in this list are the combination vibration of the C═N bond of the Schiff base. The 1624 cm^{-1} band represents its frequency in the M and with a smaller intensity in the N state and comes from the vibration of the 13 *cis* retinal. The 1639 cm^{-1} is a frequency characteristic for the bR state (Bagley et al., 1982; Smith et al., 1985; Earnest et al., 1986) and comes from the all-*trans* retinal. The rest of the bands have previously been attributed to the vibration of the protein's backbone.

The low noise content of the measurement in the amide I region resulted in very noiseless kinetics to the Gaussian amplitudes, so the deviation of the calculated Θ(*t*) values are small too (Fig. 6). The time dependence of the Θ angles (apart from the random noise) is negligible for five of these bands except for the 1652 cm^{-1} and the 1699 cm^{-1} bands. This means that the Θ value for the five bands does not change in time. The time dependence of the Θ angle in the case of the 1652 cm^{-1} and the 1699 cm^{-1} bands can be described only as a trend: the first one decreases, the second one increases, but here the increase is greatly masked by noise. There is another difference band, however, which is characteristic for the N state: the 1667 cm^{-1} band. The Gaussian amplitudes obtained from fitting this band show such time dependence that the calculation of the Θ angle is not straightforward. The behavior of these amplitudes is discussed later.

The time dependence of the Gaussian amplitude series ($A_{II}(t)$ and $A_{\perp}(t)$) in this case also was explored by fitting them to a sum of exponentials (Fig. 5, *c* and *d*). The obtained τ values were: 0.44, 2.43, and 11.74 s, which correspond well to those fitted to the time-dependent Gaussian amplitudes of the COOH bands. Table 3 shows the calculated Θ values and exponential amplitudes for the amide I bands. In the row "type" the letter "M" indicates bands that are present in the difference spectrum of the M state and are insignificant in that of the N state according to the literature, and the letter "N" indicates the ones that are present either exclusively in the spectrum of N or both in that of N and M.

Retinal Schiff base

From Table 3 it is clear that the retinal's Schiff base changes its position at one time between the bR and the M states indicated by the change of the Θ angle of the dipole moment from ~15 to ~58°. The appearance of the SB bands cannot be determined in terms of intermediate states with the present time resolution measurement. The band pair is very likely present already in the K state (Bagley et al., 1982; Weidlich and Siebert, 1993), but it surely is in the L state (Ormos et al., 1992). From this we can conclude that the two

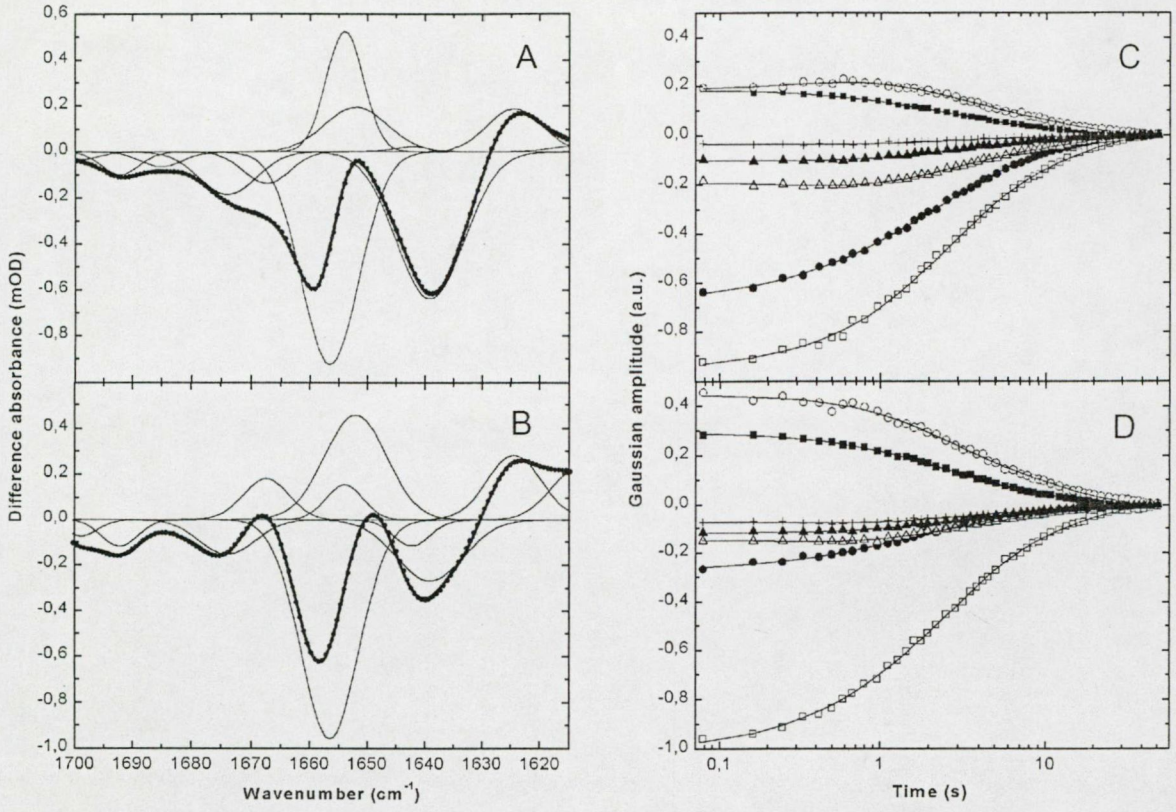

FIGURE 5 Gaussian fit to the 1613 cm^{-1} to 1704 cm^{-1} amide I region of the photoselection difference spectra measured on bR film (t = −8°C). Figures on the left (parallel polarization (*a*) and perpendicular polarization (*b*)) show the original, unsmoothed spectra 78 ms after photoexcitation (*thick line*), the fitted curve to these early spectra (*dotted line*), and the individual Gaussian components (*thin line*). Figures on the right (parallel polarization (*c*) and perpendicular polarization (*d*)) show the time evolution of the Gaussian amplitudes of the 1624 cm^{-1} (■), the 1639 cm^{-1} (●), the 1652 cm^{-1} (○), the 1657 cm^{-1} (□), the 1674 cm^{-1} (△), the 1692 cm^{-1} (▲), and the 1699 cm^{-1} (+) bands together with the exponential fit of these time dependent amplitudes (*thin line*).

bands are created not because of the deprotonation of the SB (because it deprotonates only in M) but because of the isomerization. To determine the value of Θ of the SB in an earlier protonated but already isomerized state, one needs to measure similar photoselection measurements on the K and/or L states. It is still a question of how the deprotonation (i.e., M accumulation) affects this angle. Here we can claim that in the all-*trans* protonated bR state the direction of the projection of the C=N bond's dipole makes a 15 ± 3° angle with that of the optical transition moment, and in the deprotonated 13-*cis* M state this angle is already 58 ± 2°. The two SB bands clearly belong to the "M" type according to their kinetics, in clear correspondence with papers showing that in the N spectrum these bands either are not present anymore or only with very small intensity (Pfefferlé et al., 1991; Ormos et al., 1992; Sasaki et al., 1992, 1994; Yamazaki et al., 1998).

Amide I band assignment

The rest of the bands in the amide I region originate from the C=O stretch mode of the peptide bond in the protein backbone. It has been known that these bands represent large-scale conformational changes in the protein structure. However, their assignment has not been done so far. With the results of our Θ angle measurements and by comparing them with recently published x-ray structural data (Belrhali et al., 1999 (PDB file, 1QHJ); Luecke et al., 1999 (PDB files, 1C8R and 1C8S); Luecke et al., 2000 (PDB file, 1F50); Sass et al., 2000 (PDB file, 1CWQ)), the chain segments that are responsible for these protein backbone difference bands and therefore are involved in the large-scale conformational changes in bR can be identified.

The area of the Gaussian curves corresponding to each amide I band can be used to estimate the number of groups that can be the origin of the particular IR difference band. This can be done by comparing the area of the amide I band

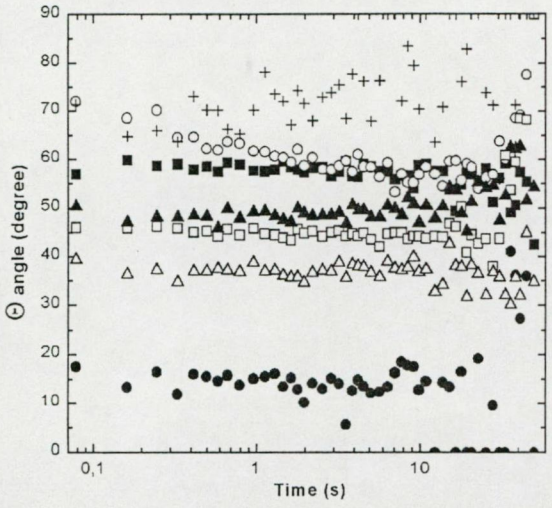

FIGURE 6 The time dependence of the angle Θ between the projection of the retinal's IR dipole moment and that of the IR dipole moments of C=O peptide groups responsible for the amide I difference bands: 1652 cm^{-1} (○), 1657 cm^{-1} (□), 1674 cm^{-1} (△), 1692 cm^{-1} (▲), and 1699 cm^{-1} (+). The Θ of the two Schiff-base bands are also shown: 1624 cm^{-1} (■) and 1639 cm^{-1} (●).

of the bR absolute absorption spectrum and the area of the chosen Gaussian. The process described below needed a separate unpolarized measurement on the same sample at the same temperature. First we assume that at saturating laser intensity at most 33% of the bR molecules is converted to M (Becher and Ebrey, 1977; Goldschmidt et al., 1977). In this experiment we used an excitation level to achieve 81% of saturation, i.e., 27% of bR was photoconverted. It was determined that the first difference spectrum taken at $t = 78$ ms contained ~90% of the M state's spectrum therefore ~24% of bR is in the M state at this time. In this spectrum the area of the Gaussian fitted to the 1657 cm^{-1} amide I band was 0.0546. The area of the entire amide I band in the absolute absorption spectrum was 32.36, this is produced by the stretching vibration of the C=O peptide bond of the 248 residues. The share of the 24% photoconverted bR molecules from the area of the total absorption band is 7.76. We also have to consider that the direction of the transition moments of the C=O bond makes an average of 35° angle with the axis of the α-helices (Marsh et al., 2000), which in our case is roughly the normal of the sample. From these data we calculated that ~5.25 amino groups are needed to produce the 1657 cm^{-1} difference band. The rest of the amide I difference bands are much smaller, so they very likely originate from single amino acids. In the case of the bands that correspond to single amino acid side chains, there is hope to identify the corresponding groups. Note that this also means an inherent limitation of the method: in cases of highly overlapping bands, assignment is not possible. Consequently, potentially "interesting" side chains may be not identified. It has to be pointed out here, too, that unambiguous assignment can be done by labeling specific groups, so the assignments done without this (like here) have to be regarded as tentative.

The existence of good quality x-ray structure of wild-type and mutant bR and the measured Θ angles form the kinetically analyzed bands made the assignment of the protein backbone bands possible. To get a more precise picture, the comparison of four ground state and two M form x-ray structures were performed in terms of the direction of the peptide C=O dipole and were used in addition for the assignment. For the assignment we used the amide band intensities together with the PDB files with the accession codes 1CWQ, 1QHJ, 1C8R, 1C8S, and 1F50. Because there are different numbers of amino acid groups in these structural models, there are regions that cannot be compared. The assignment procedure was performed as follows: as a first step of the procedure we determined the orientation of the IR transition dipole moment of the C=O stretching vibration of each peptide bond in the coordinate system of the actual x-ray structure resulting in the $M_{IR,C=O}$ vectors. In doing this, two assumptions were made: 1) the dipole moment vector is in the peptide plane and 2) the dipole moment vector makes an angle of $\delta_M = 20°$ with the direction of the C=O bond, pointing away from the N atom of the peptide bond (Marsh et al., 2000; Rothschild and Clark, 1979). The second step was to calculate the Θ angle for each dipole moment: we projected the IR dipole moment vectors

TABLE 3 Result of the Gaussian fit to the difference spectra in the amide I region

Band position	1624 cm^{-1}	1639 cm^{-1}	1652 cm^{-1}	1657 cm^{-1}	1674 cm^{-1}	1692 cm^{-1}	1699 cm^{-1}
Sign of the band	Positive	Negative	Positive	Negative	Negative	Negative	Negative
Θ Value	58 ± 2°	15 ± 3°	70–55°	45.5 ± 1.5°	37 ± 2°	49 ± 2°	65–80°
Exponential amplitudes for $A_{\parallel}$ spectra, $(a_{i,\parallel})$ i = 1, 2, 3	$a_1 = 0.006$ $a_2 = 0.119$ $a_3 = 0.063$	$a_1 = -0.102$ $a_2 = -0.415$ $a_3 = -0.157$	$a_1 = -0.096$ $a_2 = 0.135$ $a_3 = 0.142$	$a_1 = -0.016$ $a_2 = -0.646$ $a_3 = -0.296$	$a_1 = 0.069$ $a_2 = -0.142$ $a_3 = -0.113$	$a_1 = 0.017$ $a_2 = -0.077$ $a_3 = -0.044$	$a_1 = 0.009$ $a_2 = -0.029$ $a_3 = -0.015$
Exponential amplitudes for $A_{\perp}$ spectra, $(a_{i,\perp})$ i = 1, 2, 3	$a_1 = 0.005$ $a_2 = 0.197$ $a_3 = 0.094$	$a_1 = -0.051$ $a_2 = -0.164$ $a_3 = -0.059$	$a_1 = -0.024$ $a_2 = 0.262$ $a_3 = 0.212$	$a_1 = -0.076$ $a_2 = -0.639$ $a_3 = -0.291$	$a_1 = 0.044$ $a_2 = -0.102$ $a_3 = -0.088$	$a_1 = 0.015$ $a_2 = -0.080$ $a_3 = -0.053$	$a_1 = 0.025$ $a_2 = -0.052$ $a_3 = -0.045$
Type	M	M	N	M	N	N	N

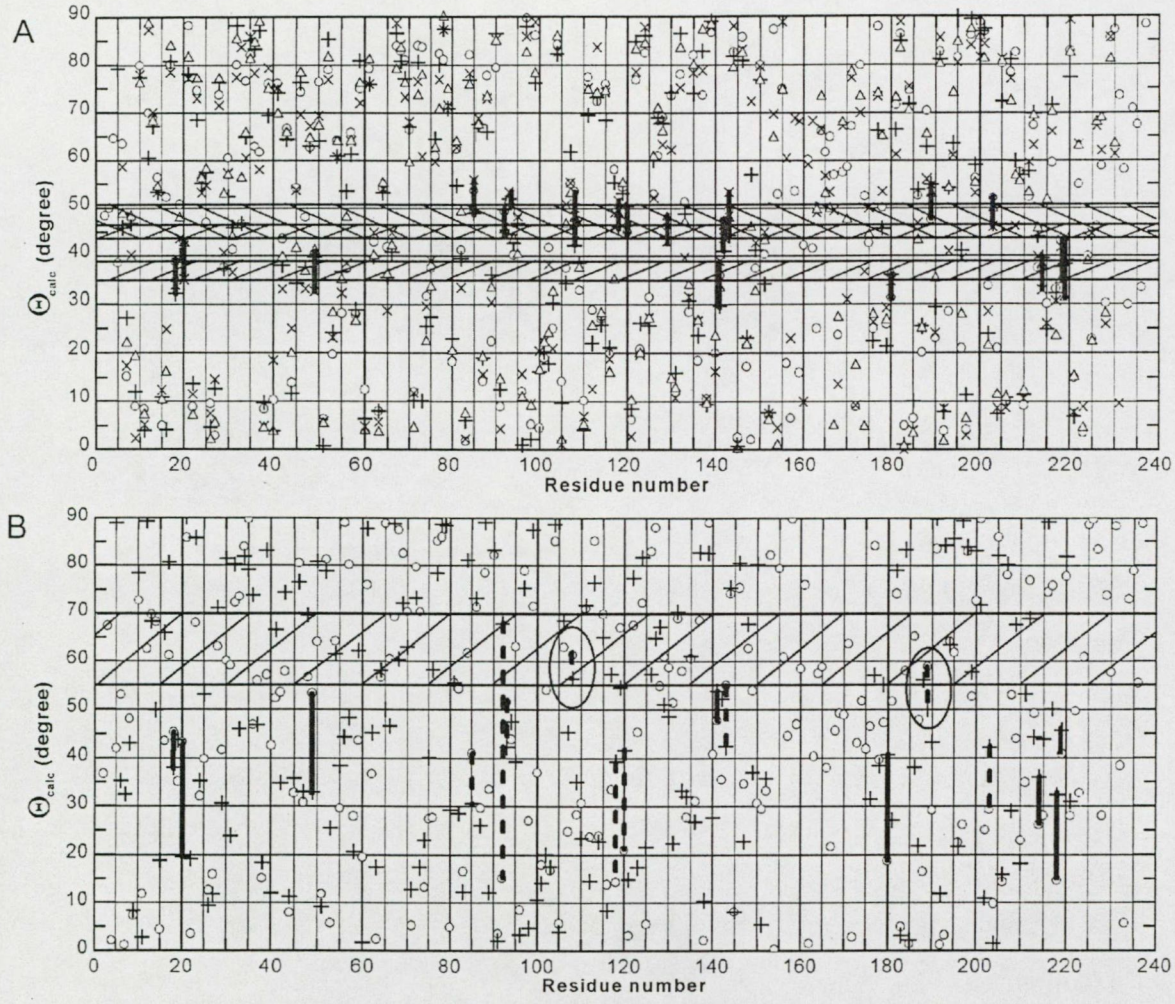

FIGURE 7 Calculated Θ_{calc} angles of the C=O peptide groups of each residue in the bR molecule in the ground state (*a*) and in the M state (*b*). Subfigure (*a*) contains angle values from four x-ray structures: ○, wild type from Sass et al. (2000); ×, wild type from Belrhali et al. (1999); +, mutant D96N from Luecke et al. (1999); and △, mutant E204Q from Luecke et al. (2000). We defined the angular regions for the amide I bands by the photoselcetion measurement: 1657 cm^{-1} band (*shaded* ××××), 1674 cm^{-1} band (shaded /), and 1692 cm^{-1} band (shaded \). The vertical bars span over the four Θ_{calc} values of the amino acid side chains that match one assignment criterium. In subfigure (*b*) only two structures are presented: ○, Sass et al. (2000); +, Luecke et al. (1999). The vertical bars cover the two Θ_{calc} values calculated for the amino acid side chains assigned to the 1674 cm^{-1} (*solid lines*) and the 1692 cm^{-1} (*dashed lines*) amide bands. Circled are the angle values of Ile-108 and Trp-189 in the M state.

($M_{IR,C=O}$) of every C=O bond and the electronic transition moment of the retinal ($M_{EL,RET}$) to the membrane plane (referred to as $m_{IR,C=O}$, and $m_{EL,RET}$, respectively), and calculated the angle between them (Θ_{calc}). We assumed that the direction of $M_{EL,RET}$ is parallel to the retinal's physical axis (Fahmy et al., 1989). Fig. 7 shows the obtained Θ_{calc} angles for the four ground state and two M state structures.

Finally, a selection was made among the amino acid side chains using the Θ_{calc} angles from the four ground state models and the measured Θ angles of the three amide I bands. The time-resolved measured Θ angle of each amide I band (1657 cm^{-1}, 1674 cm^{-1}, and 1692 cm^{-1}) has an average value in the 0 to 90° scale. When plotted against the residue serial number, the Θ_{calc} values obtained from the four models (Fig. 7) might match one of the measured Θ angles. The assignment is based on two reasonable matching criteria by which the residues are selected. First, a residue is selected if all four corresponding Θ_{calc} values from the x-ray structures are in the range defined by the minimum and the maximum of the measured Θ angle of an amide I band. Second, one is selected if two of its four Θ_{calc} values are closer to the average of the measured Θ than its deviation (±2°) and the other two are closer than 7°. This selection resulted in five groups for the 1657 cm^{-1} band,

TABLE 4 Comparison of the orientation of the amide C=O bonds obtained from FTIR experiments with X-ray structure data

IR difference band	1657 cm^{-1}	1674 cm^{-1}	1692 cm^{-1}
Amino acid side chains associated to the difference band	Leu-92 (Θ = 44.5–49.7°) Gly-120 (Θ = 45–50.4°) Lys-129 (Θ = 43.1–48°) Thr-142 (Θ = 41–47.3°) Ile-203 (Θ = 46–52°)	Ala-18 (Θ = 32.1–38.8°) Met-20 (Θ = 35–43°) Val-49 (Θ = 32.5–40.9°) Ser-141 (Θ = 29.6–38.9°) Val-180 (Θ = 31.2–36.4°) Ser-214 (Θ = 32.8–39.5°) Gly-218 (Θ = 34.7–43.2°) Phe-219 (Θ = 31.1–43.9°)	Asp-85 (Θ = 48.9–56°) Leu-92 (Θ = 44.65–49.7°) Leu-93 (Θ = 51.6–53.3°) Ile-108 (Θ = 42.2–53.2°) Met-118 (Θ = 46–51.5°) Gly-120 (Θ = 45–50.4°) Ala-143 (Θ = 44.2–53.3°) Trp-189 (Θ = 47.5–54.9°) Ile-203 (Θ = 46–52°)

eight groups for the 1674 cm^{-1} band, and nine groups for the 1692 cm^{-1} band, which are represented by vertical bars in Fig. 7 *a*.

From the bands shown in Table 3 we could choose the 1657 cm^{-1}, 1674 cm^{-1}, and 1692 cm^{-1} bands to assign to the structure because the angular range of Θ of the other two amide bands were too wide, consequently the assignment procedure yielded too many amino acid groups as possible origin of these difference bands. The fact that these three bands are negative in the difference spectrum means that their frequency represents the bR ground state. This is why we chose amino acid groups from the ground state structure Θ_{calc} to match the bands' measured Θ angle. The result of the assignment procedure is shown in Table 4.

With the reasonable assumption that the protein structure of D96N by Luecke et al. (1999) and wild type by Sass et al. (2000) after the large conformational changes represents both late M and N like structures, the assignment of the 1674 cm^{-1} and the 1692 cm^{-1} bands can be narrowed down. After the investigation of the exponential amplitudes in Table 3, one can see that kinetics of the positive band at 1652 cm^{-1} and that of the negative ones at 1674 cm^{-1} and 1692 cm^{-1} are very similar. Therefore, they can be assigned to the same transition, i.e., most likely the new position of one of the 1674 cm^{-1} and 1692 cm^{-1} bands is the 1652 cm^{-1} band in the N state. Consequently, the possible candidates for the origin of these bands have to simultaneously satisfy the orientation conditions for the ground state (Θ_{1674} = 37 ± 2° or Θ_{1692} = 49 ± 2°) and for the N state (Θ_{1652} = 62 ± 7°). Ile-108 satisfies these conditions in both structures, Ala-143 and Trp-189, only in the model of Sass et al. (2000) having lower values for N state in Luecke et al. (1999) (42° and 50°, respectively) and Leu-92 in the model of Luecke et al. (1999) owing a much lower value in Sass et al. (2000) (15°) (Fig. 7 *b*). Therefore, the best matches are Ile-108 and Trp-189. Ile-108 is at the cytoplasmic end of helix D, far from Asp-96 and the proposed proton transfer chain from Asp-96 to the Schiff base. Therefore, it possibly does not have any significant role in the function of bR. On the other hand, the rings of Trp-189 situating between Glu-194, member of the proton-release complex, and the retinal has been shown to undergo a directional change between bR and N even in the D96N mutant beside the wild type. We therefore propose that the 1692 cm^{-1} negative band shifts to the 1652 cm^{-1} positive band and tentatively assign them to a single group that is either Ile-108 or Trp-189.

The 1667 cm^{-1} band

The amplitude of the Gaussian curve fitted to the 1667 cm^{-1} band is negative for the A_{II} spectrum series but it is positive for $A_{\perp}$. This behavior is strange if we consider the calculation of the angle Θ, which requires from A_{II} and $A_{\perp}$ to have identical sign. It can be explained if we assume that the dipole moment of the C=O group, which vibrates with this frequency in the bR state, simply changes its orientation during the bR→M transition without changing its frequency. This also explains why this band is not seen in the M state in nonpolarized measurements and why it appears in polarized photoselection measurements when the parallel and perpendicular directions are measured separately (Breton and Nabedryk, 1989).

This argument is supported by kinetic calculations (Fig. 8), too. First, the amplitude of the Gaussian of this band is positive for the perpendicular polarization, and it is negative for the parallel one at the very first time slice (~78 ms after the laser flash). At this time almost exclusively the M state is present, as seen from the difference spectra. This means that in the M state, the parallel component of the absorption of this band is smaller, and the perpendicular is larger relative to that in the bR state. So in the M intermediate its frequency is the same as in bR but its orientation is not.

In the next step we fitted exponentials to the Gaussian amplitudes of the amide bands and found that the exponential amplitudes of the first time constant ($a_{1,II}$ and $a_{1,\perp}$ of τ_1 = 0.44 s) of this band have the same positive sign, but those of the second one (τ_2 = 2.42 s) are opposite: $a_{2,II}$ is negative and $a_{2,\perp}$ is positive. $a_{3,II}$ and $a_{3,\perp}$ for the 1667 cm^{-1} band have also the same sign: they are both negative. The positiveness of both a_1 amplitudes means that both the parallel and perpendicular Gaussian amplitudes decrease with the

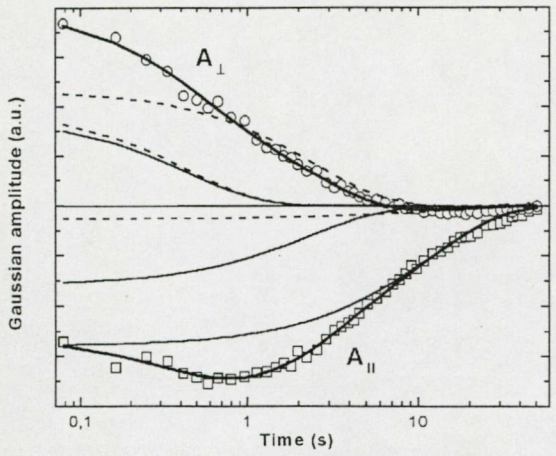

FIGURE 8 The Gaussian amplitude of the 1667 cm^{-1} band measured in parallel (□) and perpendicular (○) polarized IR light in respect to that of the actinic light. The time dependent amplitudes were fitted to a sum of exponentials (*thick line*). The individual exponential components were also calculated both in the parallel (*thin line*) and in the perpendicular (*dashed line*) cases.

first time constant. This is consistent with what we found earlier, namely, that the $\tau_1 = 0.44$-s time constant represents the M→N decay. In this frame we can explain the decrease of the Gaussian amplitude of the 1667 cm^{-1} band with $\tau_1 = 0.44$ s in the parallel (A_{II}) case to a more negative value and its concurrent decrease in the perpendicular ($A_{\perp}$) case toward zero. These decreases show that the frequency of the dipole shifts from its original value in both the bR and M states to a new value in N. The new frequency of the dipole in the N state is not known, however. We can summarize that with $\tau_1 = 0.44$ s not only the M state decays but the N builds up, which is shown by the appearance of the negative 1667 cm^{-1} band.

The question, why the positive perpendicular Gaussian amplitude of the 1667 cm^{-1} band does not become negative as well can probably be answered with the recovery of the bR state.

CONCLUSIONS

By performing polarized time resolved FTIR experiments we were able to characterize motions of the carboxylic groups, the Schiff base, and some amide I dipoles during the photocycle. Comparison of recent x-ray diffraction data with FTIR spectroscopy results helped the assignment of bands in the infrared spectra that have been intensively studied earlier in spectroscopy studies. In addition, the comparison of the data made the identification of the protonated oxygen in carboxylic groups possible. As new x-ray structure results emerge, such comparative studies should be further pursued. Time-resolved spectroscopy (both infrared and visible) yields highly detailed dynamic information about the photocycle reactions, whereas the more static x-ray structures has atomic resolution: the combination of the two approaches may result in a complete understanding of the events during function.

The authors acknowledge fruitful discussions with A. Dér, G. Groma, and G. Váró.

This work was supported by grant Országos Tudományos Kutatási Alap No. T29764.

REFERENCES

Bagley, K., G. Dollinger, L. Eisenstein, A. K. Singh, and L. Zimányi. 1982. Fourier transform infrared difference spectroscopy of bacteriorhodopsin and its photoproducts. *Proc. Natl. Acad. Sci. U.S.A.* 79:4972–4976.

Barabás, K., A. Dér, Zs. Dancsházy, P. Ormos, L. Keszthelyi, and M. Marden. 1983. Electro-optical measurements on aqueous suspension of purple membrane from *Halobacterium Halobium*. *Biophys. J.* 43:5–11.

Becher, B., and T. G. Ebrey. 1977. The quantum efficiency for the photochemical conversion of the purple membrane protein. *Biophys. J.* 17:185–191.

Belrhali, H., P. Nollert, A. Royant, C. Menzel, J. P. Rosenbusch, E. M. Landau, and E. Pebay-Peyroula. 1999. Protein, lipid and water organization in bacteriorhodopsin crystals: a molecular view of the purple membrane at 1.9 Å resolution. *Structure.* 7:909–917.

Breton, J., and E. Nabedryk. 1989. Light-induced polarized Fourier transform infrared spectroscopy of bacteriorhodopsin: a study of the M_{412} intermediate by photoselection. *Biochim. Biophys. Acta.* 973:13–18.

Czégé, J., A. Dér, L. Zimányi, and L. Keszthelyi. 1982. Restriction of motion of protein side chains during the photocycle of bacteriorhodopsin. *Proc. Natl. Acad. Sci. U.S.A.* 79:7273–7277.

Earnest, T. N., P. Roepe, M. S. Braiman, J. Gillespie, and K. J. Rothschild. 1986. Orientation of the bacteriorhodopsin chromophore probed by polarized Fourier transform infrared difference spectroscopy. *Biochemistry.* 25:7793–7798.

Fahmy, K., F. Siebert, M. F. Groβjean, and P. Tavan. 1989. Photoisomerization in bacteriorhodopsin studied by FTIR, linear dichroism and photoselection experiments combined with quantum chemical theoretical analysis. *J. Mol. Struct.* 214:257–288.

Fahmy, K., F. Siebert, and P. Tavan. 1991. Structural investigation of bacteriorhodopsin and some of its photoproducts by polarized Fourier transform infrared spectroscopic methods-difference spectroscopy and photoselection. *Biophys. J.* 60:989–1001.

Gerwert, K., G. Souvignier, and B. Hess. 1990. Simultaneous monitoring of light-induced changes in protein side-group protonation, chromophore isomerization, and backbone motion of bacteriorhodopsin by time-resolved Fourier-transform infrared spectroscopy. *Proc. Natl. Acad. Sci. U.S.A.* 87:9774–9778.

Goldschmidt, C. R., O. Kalisky, T. Rosenfeld, and M. Ottolenghi. 1977. The quantum efficiency of the bacteriorhodopsin photocycle. *Biophys. J.* 17:179–183.

Hatanaka, M., H. Kandori, and A. Maeda. 1997. Localization and orientation of functional water molecules in bacteriorhodopsin as revealed by polarized Fourier transform infrared spectroscopy. *Biophys. J.* 73: 1001–1006.

Heberle, J. 2000. Proton transfer reactions across bacteriorhodopsin and along the membrane. *Biochim. Biophys. Acta.* 1458:135–147.

Heyn, M. P., and H. Otto. 1992. Photoselection and transient linear dichroism with oriented immobilized purple membranes: evidence for motions of the C(20)-methyl group of the chromophore towards the cytoplasmic side of the membrane. *Photochem. Photobiol.* 56: 1105–1112.

Kandori, H. 1998. Polarized FTIR spectroscopy distinguishes peptide backbone changes in the M and N photointermediates of bacteriorhodopsin. *J. Am. Chem. Soc.* 120:4546–4547.

Ludmann, K., Cs. Gergely, A. Dér, and Gy. Váró. 1998. Electric signals during the bacteriorhodopsin photocycle, determined over a wide pH range. *Biophys. J.* 75:3120–3126.

Luecke, H., B. Schobert, J.-P. Cartailler, H.-T. Richter, A. Rosengarth, R. Needleman, and J. K. Lanyi. 2000. Coupling photoisomerization of retinal to directional transport in bacteriorhodopsin. *J. Mol. Biol.* 300: 1237–1255.

Luecke, H., B. Schobert, H.-T. Richter, J.-P. Cartailler, and J. K. Lanyi. 1999. Structural changes in bacteriorhodopsin during ion transport at 2 Angstrom resolution. *Science.* 286:255–260.

Marsh, D., M. Müller, and F.-J. Schmitt. 2000. Orientation of the infrared transition moments for an α-helix. *Biophys. J.* 78:2499–2510.

Nabedryk, E., and J. Breton. 1986. Polarized Fourier transform infrared (FTIR) difference spectroscopy of the M_{412} intermediate in the bacteriorhodopsin photocycle. *FEBS Lett.* 202:356–360.

Oesterhelt, D., and W. Stoeckenius. 1974. Isolation of the cell membrane of *Halobacterium halobium* and its fractionation into red and purple membrane. *Methods Enzymol.* 31:667–668.

Ormos, P. 1991. Infrared spectroscopic demonstration of a conformational change in bacteriorhodopsin involved in proton pumping. *Proc. Natl. Acad. Sci. U.S.A.* 88:473–477.

Ormos, P., K. Chu, and J. Mourant. 1992. Infrared study of the L, M, and N intermediates of bacteriorhodopsin using the photoreaction of M. *Biochemistry.* 31:6933–6937.

Pfefferlé, J.-M., A. Maeda, J. Sasaki, and T. Yoshizawa. 1991. Fourier transform infrared study of the N intermediate of bacteriorhodopsin. *Biochemistry.* 30:6548–6556.

Rammelsberg, R., G. Huhn, M. Lübben, and K. Gerwert. 1998. Bacteriorhodopsin's intramolecular proton-release pathway consists of a hydrogen-bonded network. *Biochemistry.* 37:5001–5009.

Rothschild, K. J., and N. A. Clark. 1979. Polarized infrared spectroscopy of oriented purple membrane. *Biophys. J.* 25:473–488.

Rothschild, K. J., T. Marti, S. Sonar, Y.-W. He, P. Rath, W. Fischer, and H. G. Khorana. 1993. Asp96 deprotonation and transmembrane α-helical structural changes in bacteriorhodopsin. *J. Biol. Chem.* 268: 27046–27052.

Sasaki, J., J. K. Lanyi, R. Needleman, T. Yoshizawa, and A. Maeda. 1994. Complete identification of C = O stretching vibrational bands of protonated aspartic acid residues in the difference infrared spectra of M and N intermediates versus bacteriorhodopsin. *Biochemistry.* 33:3178–3184.

Sasaki, J., Y. Shichida, J. K. Lanyi, and A. Maeda. 1992. Protein changes associated with reprotonation of the Schiff-base in the photocycle of Asp96→Asn bacteriorhodopsin. *J. Biol. Chem.* 267:20782–20786.

Sass, H. J., G. Büldt, R. Gessenich, D. Hehn, D. Neff, R. Schlesinger, J. Berendzen, and P. Ormos. 2000. Structural alterations for proton translocation in the M state of wild-type bacteriorhodopsin. *Nature.* 406: 649–652.

Smith, S. O., A. B. Myers, R. A. Mathies, J. A. Pardoen, C. Winkel, E. M. M. van den Berg, and J. Lugtenburg. 1985. Vibrational analysis of the all-*trans* retinal protonated Schiff-base. *Biophys. J.* 47:653–664.

Váró, Gy. and J. K. Lányi. 1991. Thermodynamics and energy coupling in the bacteriorhodopsin photocycle. *Biochemistry.* 30:5016–5022.

Weidlich, O., and F. Siebert. 1993. Time-resolved step-scan FT-IR investigations of the transition from KL to L in the bacteriorhodopsin photocycle: identification of chromophore twists by assigning hydrogen-out-of-plane (HOOP) bending vibrations. *Appl. Spectr.* 47:1394–1400.

Yamazaki, Y., H. Kandori, R. Needleman, J. K. Lanyi, and A. Maeda. 1998. Interaction of the protonated Schiff-base with the peptide backbone of Valine 49 and the intervening water molecule in the N photointermediate of bacteriorhodopsin. *Biochemistry.* 37:1559–1564.

Formation of a New Buried Charge Drives a Large-Amplitude Protein Quake in Photoreceptor Activation†

Aihua Xie,*,‡ Lorand Kelemen,‡,§ Johnny Hendriks,∥ Brandy J. White,‡ Klaas J. Hellingwerf,∥ and Wouter D. Hoff⊥

Department of Physics, Oklahoma State University, 145 Physical Sciences II, Stillwater, Oklahoma 74078, Department of Microbiology, University of Amsterdam, Nieuwe Achtergracht 166, 1018 WS Amsterdam, The Netherlands, and Department of Biochemistry and Molecular Biology, The University of Chicago, Chicago, Illinois 60637

Received October 23, 2000; Revised Manuscript Received December 15, 2000

ABSTRACT: Photoactive yellow protein (PYP) is a eubacterial photoreceptor and a structural prototype of the PAS domain superfamily of receptor and regulatory proteins. We investigate the activation mechanism of PYP using time-resolved Fourier transform infrared (FTIR) spectroscopy. Our data provide structural, kinetic, and energetic evidence that the putative signaling state of PYP is formed during a large-amplitude protein quake that is driven by the formation of a new buried charge, COO^- of the conserved Glu46, in a highly hydrophobic pocket at the active site. A protein quake is a process consisting of global conformational changes that are triggered and driven by a local structural "fault". We show that large, global structural changes take place after Glu46 ionization via intramolecular proton transfer to the anionic *p*-coumarate chromophore, and are suppressed by the absence of COO^- formation in the E46Q mutant. Our results demonstrate the significance of buried charge formation in photoreceptor activation. This mechanism may serve as one of the general themes in activation of a range of receptor proteins. In addition, we report the results of time-resolved FTIR spectroscopy of PYP crystals. The direct comparison of time-resolved FTIR spectroscopic data of PYP in aqueous solution and in crystals reveals that the structure of the putative signaling state is not developed in $P6_3$ crystals. Therefore, when the structural developments during the functional process of a protein are experimentally determined to be very different in crystals and solutions, one must be cautious in drawing conclusions regarding the functional mechanism of proteins based on time-resolved X-ray crystallography.

Embedding a charged group inside a protein in a nonpolar (low-dielectric) environment is energetically unfavorable. Therefore, most charged groups in a protein are solvent-exposed. Buried charges are unique and generally well conserved, indicating their structural and functional importance. To lower the electrostatic energy for embedding a charged group inside a protein, a buried charge must be stabilized through a network of polar groups, hydrogen bonding, and salt bridge interactions (*1*). Buried charges are important in protein folding (*1*, *2*). During the functional process of a protein, proton transfer events may lead to the formation of a new buried charge. Such a relocation of a buried charge in a protein may demand a new protein conformation. Although there are many studies on proton transfer events in energy transduction, formation of a new buried charge in triggering large conformational changes in a protein has not received significant attention. Here we show that formation of a new buried charge drives a large-amplitude protein quake that leads to PYP[1] photoreceptor activation. A protein quake (*3*) is a process consisting of global conformational changes that are triggered and driven by a local structural "fault".

PYP is a structural prototype of the PAS domain superfamily (*4*, *5*) of receptor and regulatory proteins from all three kingdoms of life. As a small water soluble photoreceptor (*6*−*8*), PYP bears a unique thioester-linked *p*-coumaric acid (pCA) chromophore (*9*, *10*) for light detection. Photoexcitation of the initial receptor state, pG_{446} (peak absorption at 446 nm), leads to a photocycle (*6*, *11*, *12*) that involves at least two intermediate states, pR_{465} (λ_{max} = 465 nm) and pB_{355} (λ_{max} = 355 nm), from 5 ns until the completion of the PYP photocycle in a few seconds. The long-lived pB_{355} state is the putative signaling state of PYP.

To investigate the molecular mechanism of PYP photoreceptor activation, we have performed time-resolved Fourier

† This work was supported by ONR Grant N00014-98-1-0854 and OCAST Fund HR98-24 to A.X., grants from the American Cancer Society (IRG-41-40) and the Cancer Research Foundation (19428) to W.D.H., and grants from the Netherlands Organization for Scientific Research (330-031/D97) and the Netherlands Foundation for Chemical Research to K.J.H.

* To whom correspondence should be addressed. E-mail: aihua@westlake.phy.okstate.edu. Telephone: (405) 744-3416. Fax: (405) 744-6811.

‡ Oklahoma State University.

§ Present address: Biological Research Centre, Institute of Biophysics, Szeged H-6726, Hungary.

∥ University of Amsterdam.

⊥ The University of Chicago.

[1] Abbreviations: PYP, photoactive yellow protein; pG_{446}, initial receptor state with peak absorption (λ_{max}) at 446 nm; pR_{465}, red-shifted photocycle intermediate with a λ_{max} of 465 nm; pB_{355}, blue-shifted photocycle intermediate with a λ_{max} of 355 nm; pCA, *p*-coumaric acid (4-hydroxycinnamic acid); FTIR, Fourier transform infrared; CaF_2, calcium fluoride; PAS, originated from signaling proteins of "PER" (periodic clock protein), "ARNT" (aryl hydrocarbon receptor nuclear translator), and "SIM" (single-minded protein); bR, bacteriorhodopsin.

10.1021/bi002449a CCC: $20.00
Published on Web 01/18/2001

transform infrared (FTIR) spectroscopic measurements of the infrared difference spectra between the photocycle intermediates and the receptor state from 10 μs to the completion of the PYP photocycle. We have identified five major spectral markers that are sensitive to crucial structural changes. These spectral markers are employed to probe the kinetics and the nature of structural transitions that result in PYP photoreceptor activation.

MATERIALS AND METHODS

Sample Preparation. Purified proteins of wild-type PYP (wt-PYP) and the E46Q mutant were obtained using the method previously reported (*13*). PYP samples for FTIR experiments were prepared with a protein concentration of approximately 10 mM in 100 mM potassium phosphate buffer in D_2O at pH* 7.0. This was achieved by dissolving about 3 mg of purified and freeze-dried PYP in 300 μL of the above buffer, and washing it three times through Microcon centrifuge filters at 14000*g*. Each solution sample was made by sandwiching 2.5 μL of the PYP solution between two CaF_2 plates 25 mm in diameter and 2 mm thick using a 12 μm spacer. The $P6_3$ PYP crystals were grown using the reported protocol (*14*). PYP crystal samples for FTIR experiments were made from polycrystals gently ground between two CaF_2 plates without a spacer. With polycrystals, the sample is effectively isotropic, so the detected signals are averaged over all crystal orientations. The kinetics of polycrystalline PYP samples were tested using time-resolved visible absorption spectroscopy, and were found to be faster than those in solution, in agreement with the reported kinetic measurement of PYP single $P6_3$ crystals using visible absorption spectroscopy (*15*).

Time-Resolved FTIR Spectroscopy. A Bruker IFS 66v FTIR spectrometer was utilized for time-resolved measurements in the spectral range of 1900−970 cm^{-1}. The PYP photocycle was triggered using laser pulses with a pulse duration of 4 ns and an energy of 6 mJ at 450 nm for wt-PYP and 430 nm for the E46Q mutant (Continuum Surelite-II pumped OPO laser). The laser repetition rate was 0.5 Hz. The laser beam size at the samples was 6 mm in diameter. The pR_{465} to pB_{355} transition in aqueous wt-PYP was probed from 10 μs to 7 ms using time-resolved step-scan FTIR spectroscopy with a time resolution of 10 μs and a spectral resolution of 4 cm^{-1}. The pB to pG transitions in aqueous wt-PYP, the E46Q mutant, and the $P6_3$ crystals of wt-PYP were monitored from 60 ms to 2 s using time-resolved rapid-scan FTIR spectroscopy with a time resolution of 60 ms and a spectral resolution of 4 cm^{-1}. The heating effect on PYP crystals was less than 2 K based on 90% absorption of laser pulse energy.

Data Analysis. All time-resolved FTIR difference spectra were calculated using the preflash data (pG_{446}) as a baseline, and averaged over repetitive measurements. The time-resolved step-scan FTIR spectra at 25 μs, 100 μs, 400 μs, 1.6 ms, and 6.6 ms (Figure 1A) were further averaged over 2, 4, 16, 64, and 256 time points, respectively, around the specified times. The kinetic data of each peak (Figure 1B) were averaged to a quasi-logarithmic base with four data points per doubling time. The pB_{355} − pG_{446} spectra (Figure 3) of wt-PYP, the E46Q mutant, and PYP in $P6_3$ crystals were the first time slices (60 ms) of the corresponding time-resolved rapid-scan FTIR data sets. The FTIR difference spectra of pR_{465}, pB'_{355}, and pB_{355} [$\Delta A_{pR}(\nu) = A_{pR}(\nu) - A_{pG}(\nu)$, $\Delta A_{pB'}(\nu)$, and $\Delta A_{pB}(\nu)$] were extracted from the experimental data of time-resolved step-scan FTIR difference spectra, $\Delta A(t,\nu)$, using the equation $\Delta A(t,\nu) = p_{pR}(t)\Delta A_{pR}(\nu) + p_{pB'}(t)\Delta A_{pB'}(\nu) + p_{pB}(t)\Delta A_{pB}(\nu)$. The population accumulations of photocycle intermediates pR_{465}, pB'_{355}, and pB_{355} [$p_{pR}(t)$, $p_{pB'}(t)$, and $p_{pB}(t)$, respectively] were calculated on the basis of a unidirectional unbranched photocycle model ($pR_{465} \rightarrow pB'_{355} \rightarrow pB_{355} \rightarrow pG_{446}$) with time constants of 260 μs, 2.0 ms, and 350 ms, respectively. The extracted pB_{355} − pG_{446} spectrum (Figure 1C) is found to be essentially identical to the one (Figure 3) directly obtained from time-resolved rapid-scan FTIR measurements at 60 ms following laser excitation, when only pB_{355} and pG_{446} are populated. This demonstrates the reliability of our spectral calculations described here.

Calculation of the Electrostatic Energy for a Buried Charge. The electrostatic energy U (*16*), which is stored in an electric field generated by a small charged group with a net charge q and a dipole moment p in a homogeneous spherical shell of a dielectric medium with an inner radius R and a thickness D, is

$$U = \frac{1}{8\pi\epsilon_0\epsilon}\left[q^2\left(\frac{1}{R} - \frac{1}{R+D}\right) + \frac{2p^2}{3}\left(\frac{1}{R^3} - \frac{1}{(R+D)^3}\right)\right]$$

where ϵ_0 (=8.85 $C^2\ N^{-1}\ m^{-2}$) is the permittivity of vacuum and ϵ is the dielectric constant. The prefactor ($1/4\pi\epsilon_0$) has a value of 14.4 eV, or 1524 kJ/mol. To the first order of approximation, this electrostatic energy due to a COO^- group in a dielectric medium is calculated using an R of 2.50 Å and a D of 4.00 Å for the first shell of atoms surrounding the COO^- group, based on the Glu46 in the PYP crystal structure. The value of D is obtained on the basis of the diameters of C and O atoms plus the effects of hydrogen atoms and the nonequal distances from the center of the COO^- group. The value of R is obtained from the average interatomic distances (4.5 Å) between the center of the COO^- group of Glu46 and the 13 neighboring atoms that form the first shell of the binding pocket (with $R + D/2 = 4.5$ Å) based on the crystal structure of pG_{446} (*14*). To calculate the electrostatic energy difference (ΔU) between the same charged group at two different binding sites in a protein, the contributions to ΔU from the first shells of atom that define the properties of the two binding pockets (e.g., hydrophilic and hydrophobic) are dominant, while the regions beyond the first shells contain many more atoms per shell and are much less different on average. As a result, their contributions to ΔU are small and not accounted for in our calculation.

RESULTS AND DISCUSSION

Time-resolved FTIR spectroscopy is a powerful technique that provides both excellent time resolution (*17*) and high structural sensitivity (*18*). We employed this technique to probe chromophore photoisomerization, proton transfer, and global conformational changes involving the protein backbone and environments of polar side chain groups during the PYP photocycle. The E46Q mutant was studied in an effort to clarify the role of buried charge formation in PYP

activation. In addition, time-resolved FTIR spectroscopy is applicable to proteins both in solutions and in crystals. We have examined the structural developments during the PYP photocycle in $P6_3$ crystals using time-resolved rapid-scan FTIR spectroscopy.

Time-resolved FTIR difference spectra between the photocycle intermediates and pG_{446} (Figure 1A) reveal progressive structural changes in PYP from 25 μs to 6.6 ms following photoexcitation. Positive bands arise from photocycle intermediates, whereas negative ones arise from pG_{446}. Only structurally active groups during the PYP photocycle are detected in the time-resolved FTIR difference spectra. Those structural groups that do not undergo any structural changes make no contribution to the difference spectra. We have identified five spectral markers for probing important structural changes during PYP activation. The 1726 cm^{-1} band is assigned to the COOD group of Glu46 (*13*). The bands at 1498 and 1514 cm^{-1} are attributed to the phenolic ring vibration of the ionized and neutral pCA chromophore, respectively (unpublished results). The positive band centered at 1624 cm^{-1} arises predominantly from the C=O stretching of the protein backbone (amide I) in antiparallel β-structure (*19*, *20*). The 1689 cm^{-1} band is due to a ND-containing side chain group (Arg, Asn, or Gln), based on its sensitivity to ^{15}N isotopic labeling and to H−D exchange (unpublished results). The region between 1610 and 1560 cm^{-1} is largely attributed to various polar side chain groups containing double bonds (*21*).

To resolve the temporal order and kinetics of key structural events during the pR_{465} to pB_{355} transition, we have analyzed the kinetics (Figure 1B) of chromophore protonation [(■) characteristic upshift of the pCA ring vibration from 1498 to 1514 cm^{-1}] (unpublished results), Glu46 ionization [(□) depletion of the 1726 cm^{-1} band] (*13*), protein conformational changes at amide I [(○) increase in the intensity of the 1624 cm^{-1} band] (*19*), and a side chain [(●) depletion of the 1689 cm^{-1} band] (unpublished results). We found that the pR_{465} to pB_{355} transition is biphasic. The fast phase (τ_1 = 260 μs) predominantly encompasses pCA protonation and Glu46 ionization, while the slow phase (τ_2 = 2 ms) primarily involves large conformational changes in PYP. The data unambiguously demonstrate that a new buried charge, COO^- of Glu46, is formed prior to large global conformational changes.

The biphasic kinetics of the pR_{465} to pB_{355} transition reveal a new photocycle intermediate, pB'_{355}. The pB'_{355} state serves as an important structural link between pR_{465} and pB_{355}, and is critical for understanding the mechanism of signaling state formation. The pB'_{355} − pG_{446} spectrum (Figure 1C) shows that in pB'_{355}, Glu46 is ionized (bleaching at 1728 cm^{-1}), the pCA is protonated (peak shift from 1498 to 1514 cm^{-1}), and the conformation of pB'_{355} strongly resembles that of pG_{446} (minimal changes in amide I and in side chain groups). The COOD group in pG_{446} is buried in a highly hydrophobic environment (Figure 2), confined by the rigid and nonpolar side chain groups of Ile31, Ile49, and Val122. Since the conformation of pB'_{355} closely resembles that of pG_{446} (Figure 1C) and the binding pocket of the COOD group of Glu46 in pG_{446} is very rigid, we therefore conclude that the newly formed charge, COO^- of Glu46, in pB'_{355} remains in its highly hydrophobic environment, and is energetically unstable.

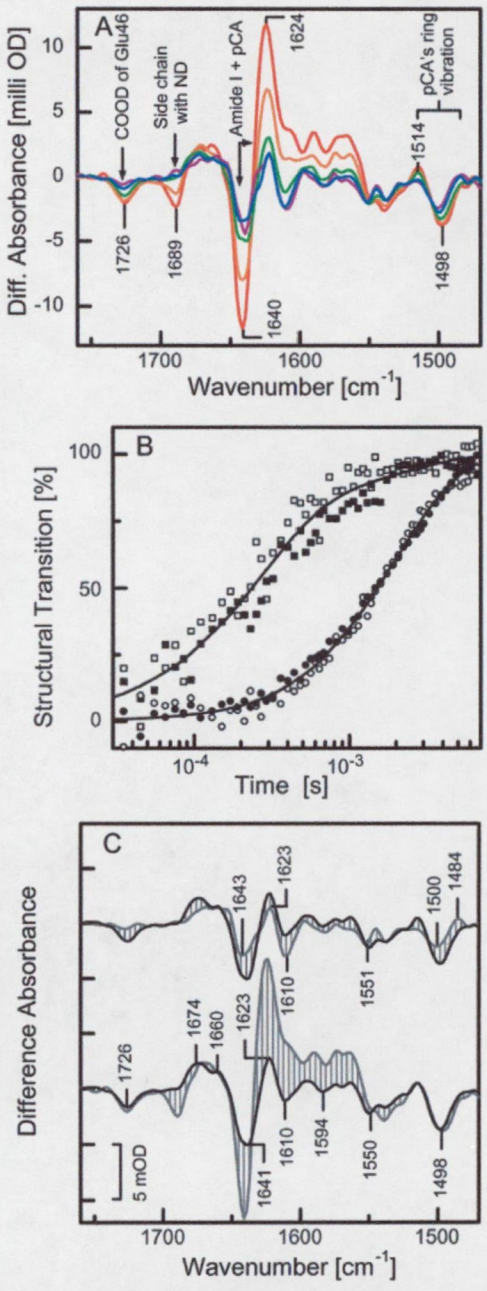

FIGURE 1: Time-resolved FTIR spectroscopy of the PYP photocycle. (A) Time-resolved FTIR difference spectra of wt-PYP at pH* 7 in D_2O at 25 μs (purple), 100 μs (blue), 400 μs (green), 1.6 ms (orange), and 6.6 ms (red). (B) The temporal courses of key structural events during the PYP photocycle: pCA protonation (■, 1498 cm^{-1}), Glu46 ionization (□, 1726 cm^{-1}), protein secondary structural changes (○, 1624 cm^{-1}), and dramatic changes in the environment of a ND-containing side chain (●, 1689 cm^{-1}). Nonlinear least-squares fitting (—) of the data to two-exponential kinetics yields a τ_1 of 260 μs and a τ_2 of 2.0 ms. The time constant for the fast kinetics is in agreement with the decay of pR from previous studies at neutral pH and room temperature (*6*, *11*). (C) Difference infrared spectra of pR_{465} (gray, top), pB'_{355} (black, top and bottom), and pB_{355} (gray, bottom) with respect to pG_{446}. The shaded areas represent the extent of structural changes during the pR_{465} to pB'_{355} transition (top) and the pB'_{355} to pB_{355} transition (bottom).

Glu46 Is the Proton Donor for Chromophore Protonation. In pG_{446}, the COOH group of Glu46 is hydrogen bonded to the negatively charged phenolic oxygen of the chromophore

(*13*, *14*). This hydrogen bond may be disrupted in pR_{465} due to chromophore photoisomerization. It was found that this bond is intact in pR_{465} at 80 K (FTIR difference spectroscopy) (*13*), but broken in pR_{465} at room temperature (nanosecond time-resolved X-ray crystallography) (*22*). This issue is crucial to understanding the proton transfer pathway for PYP activation.

Our time-resolved FTIR spectroscopic data of the PYP photocycle at room temperature unambiguously determine the hydrogen bonding status of Glu46 in pR_{465}. The COOD stretching frequency of Glu46 would be shifted from 1726 cm^{-1} in pG_{446} to approximately 1750 cm^{-1} upon loss of the hydrogen bond (*23*) or to $\leq$1600 cm^{-1} upon ionization (*21*). The $pR_{465} - pG_{446}$ spectrum (Figure 1C) reveals that (i) the carboxylic group of Glu46 remains protonated in pR_{465} (no depletion of the 1726 cm^{-1} band), (ii) the COOD group of Glu46 is unperturbed in pR_{465} (no significant peak shifts of the 1726 cm^{-1} band), and (iii) the protein conformation of pR_{465} remains unchanged from that of pG_{446} (a small peak at 1623 cm^{-1} arises from the chromophore due to photoisomerization, unpublished results). In addition, there is no alternative hydrogen bond partner for the COOD group of Glu46 within 4 Å (*14*). Therefore, the COOD group of Glu46 remains neutral and hydrogen bonded to the phenolic oxygen of the chromophore in pR_{465}.

Furthermore, pCA protonation and Glu46 ionization take place with identical kinetics (Figure 1B) with essentially no associated protein conformational changes (Figure 1C). We therefore conclude that a direct intramolecular proton transfer takes place from the COOD group of Glu46 to the negatively charged phenolic oxygen of the pCA chromophore during the pR_{465} to pB'_{355} transition.

It is intriguing that protonation of the chromophore in the E46Q mutant is 5 times faster than in wt-PYP at neutral pH (*24*). However, this does not provide informative evidence against the role of Glu46 as the proton donor for pCA in wt-PYP. First, the chromophore in the E46Q mutant may be protonated by direct proton transfer via a hydrogen-bonded wire (*25*) involving the OH groups of Tyr42 and Thr50, when the primary proton donor, COOH of Glu46, is absent. Second, the rate of this secondary protonation pathway may be increased due to an increased proton affinity of the chromophore caused by the E46Q mutation. It is important to point out that the electronic state of the pCA chromophore is perturbed by the E46Q mutation, as observed from changes in the peak positions and amplitudes of the chromophore vibration bands (Figure 3A) and a significant red shift of the visible peak absorption (*24*, *26*) from 446 nm in wt-PYP to 462 nm in the E46Q mutant. In addition, the faster protonation of the chromophore in the E46Q mutant can also be due to a reduced energy barrier for the pR to pB′ transition, since pB′ in the mutant is formed without creating a new buried charge at the hydrophobic binding site. Finally, our observation that the E46Q mutation greatly reduces the extent of structural changes during the formation of the pB-like state (see Figure 3 and below) fully supports the role of Glu46 as the proton donor in wt-PYP and its importance in PYP activation.

Formation of a New Buried Charge, COO^- of Glu46, Drives Large Conformational Changes. Extensive evidence showing that the protein conformation of the putative signaling state, pB_{355}, is largely different from that of pG_{446} has been reported (*27*, *28*). Comparison of the infrared difference spectra of pR_{465}, pB'_{355}, and pB_{355} (Figure 1C) reveals that such large conformational changes take place during the pB'_{355} to pB_{355} transition. The large positive amplitude of the spectral marker at 1624 cm^{-1} in the $pB_{355} - pG_{446}$ spectrum evidences large structural changes in the protein secondary structure. The spectral marker for the polar side chain groups with double bonds (1610−1560 cm^{-1}) exhibits four positive bands, indicating changes in the environment of four polar side chain groups. Exposed polar and charged groups are not expected to contribute to the difference spectra as long as they remain exposed. There are 12 buried and partially buried polar groups in pG_{446} (*14*). Therefore, the data indicate that the large global conformational changes during the pB'_{355} to pB_{355} transition involve one-third of the buried and partially buried groups. The molecular mechanism for PYP activation has been disputed (*13*, *27*, *29*). We present the following strong evidence for the decisive role of Glu46 ionization in driving signaling state formation.

The COO^- group of Glu46 in pB'_{355} is embedded in a highly hydrophobic environment (Figure 2). Buried charges in hydrophobic interiors of proteins exert strong destabilizing effects on protein structures (*1*, *2*). We show a method (see Materials and Methods) for estimating the electrostatic energy difference between a buried COO^- group in a highly hydrophobic environment (with a dielectric constant ϵ of 2.5) and the same group in a less hydrophobic or hydrophilic environment (ϵ of 5−7) in proteins. Using a charge q of −0.80 e and a dipole moment p of 1.00 eÅ from our ab initio Gaussian98 calculation or the larger values of q (−1.0 e) and p (1.3 eÅ) for the COO^- group, the electrostatic energy difference is found to be 28−55 kJ/mol. In comparison, a typical value for protein folding energy is approximately 40 kJ/mol (*2*). Therefore, the destabilizing electrostatic energy of this single buried COO^- group of Glu46 in pB'_{355} is sufficiently strong to drive large conformational changes during pB_{355} formation.

The electrostatic energy of a buried charge is determined by two effects (*16*): the effective radius of the charge and the effective dielectric constant of its environment (see Materials and Methods). Both effects contribute to an increased electrostatic energy upon the pG_{446} to pB'_{355} transition. The negative charge on the pCA chromophore in pG_{446} is more delocalized via conjugated electrons (larger effective radius) than the charge on the COO^- group of Glu46 in pB'_{355}. In addition, the binding pocket of the pCA (Figure 2) in pG_{446} and pR_{465} is less hydrophobic with 40% polar atoms (nine oxygens, eight nitrogens, and one sulfur) and 60% nonpolar atoms (29 carbons) than the binding pocket of the COO^- of Glu46 in pB'_{355} with 17% polar atoms (two oxygens) and 83% nonpolar atoms (11 carbons).

To experimentally investigate the role of creating a new buried charge, COO^- of Glu46, in driving large conformational changes, we performed time-resolved FTIR spectroscopy on the photocycle of the E46Q mutant, in which formation of a new buried charge (COO^-) is abolished. A pB-like state is formed during the photocycle of the E46Q mutant (*24*). This pB state was identified by visible absorption spectroscopy, which is a local probe only sensitive to the pCA chromophore, not to the entire protein. In contrast, time-resolved FTIR spectroscopy is sensitive to the structure

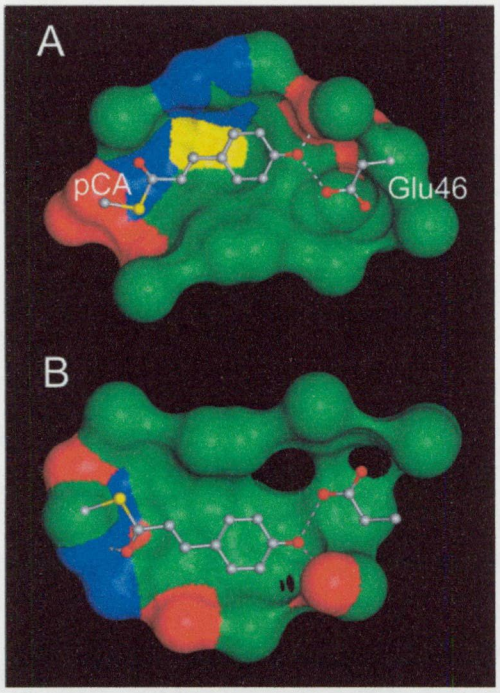

FIGURE 2: Electrostatic properties of the binding pocket for the pCA chromophore and the COOH group of Glu46 in pG_{446}. The binding pocket is formed from the atoms on the first shell, and is depicted as a surface generated using a probe with a 1.6 Å radius. The top half of the binding pocket (A) is formed, for pCA, from the atoms of Tyr42 (OH, CZ), Thr50 (OG1, CB, CG2), Arg52 (NH1, NH2, CZ, NE, CD), Tyr94 (CE2), Thr95 (O), Phe96 (C, CA, CB, CD1, CD2, CE1, CE2, CG, CZ), Asp97 (N, OD1, OD2), Tyr98 (N, CB), and Met100 (SD) and, for the carboxylic group of Glu46, from the atoms of Gly29 (CA), Glu46 (CA, O), Ile49 (CB, CD1, CG2), and Val122 (CG1). The bottom half of the binding pocket (B) is formed, for pCA, from the atoms of Ile31 (CD1), Tyr42 (OH, CZ, CE2), Phe62 (CZ, CE1), Val66 (CG1, O), Ala67 (CA, CB, O), Pro68 (N), Cys69 (CA, N, O), Thr70 (CG2, N), Tyr94 (CE2), and Phe96 (CZ, CE1) and, for the COOH group of Glu46, from the atoms of Gly29 (C, CA), Ile31 (CD1, CG1), and Val122 (CG1, CG2). The green areas (carbon) represent a low-dielectric medium, whereas red (oxygen), blue (nitrogen), and yellow (sulfur) areas denote a high-dielectric environment. The chromophore and the side chain group of Glu46 are illustrated in sticks and balls, with gray for carbon, red for oxygen, and yellow for sulfur. Three hydrogen bonds are shown as dashed lines. Since the binding pocket of the COOH group of Glu46 is very rigid in pG_{446} and the structural fold of pB'_{355} is very similar to that of pG_{446}, the binding pocket for the COO^- group of Glu46 in pB'_{355} is expected to be very similar to that in pG_{446} as illustrated here.

of both the chromophore and the entire protein. The pB − pG FTIR difference spectrum of the E46Q mutant (Figure 3A) reveals that the intensities of the amide I signals, probing the backbone structural changes, are dramatically reduced in the E46Q mutant compared with that of wt-PYP, and that the strong 1689 cm^{-1} band for a side chain group in wt-PYP is not present in the E46Q mutant. Therefore, the extent of conformational changes from pG to pB is greatly reduced in the E46Q mutant. This result demonstrates that the protonation of the chromophore by itself has little effect on the protein conformation. It is the formation of a new buried charge, COO^- of Glu46, that drives large conformational changes.

Importance and Limitations of Time-Resolved X-ray Crystallography. X-ray crystallography of static proteins is the most powerful technique for resolving the three-

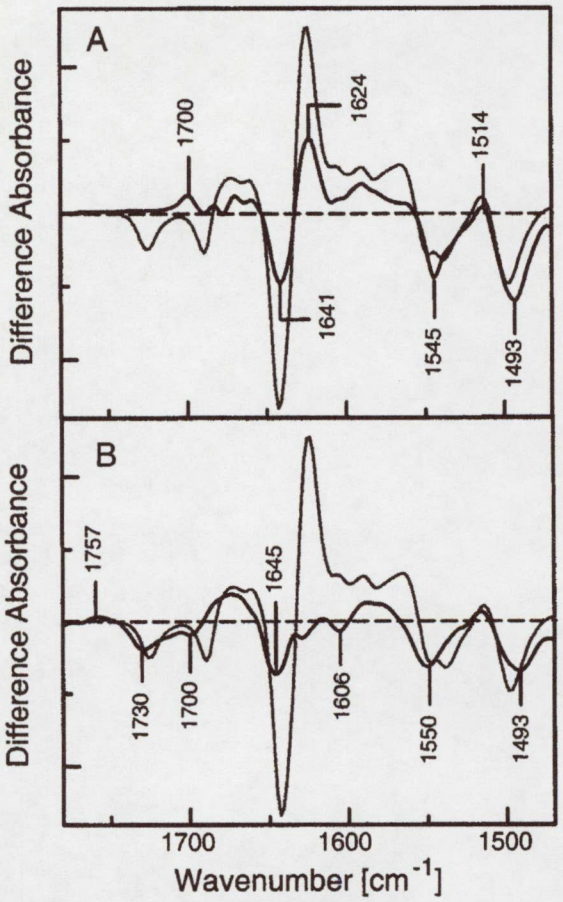

FIGURE 3: pB − pG infrared spectra of the E46Q mutant (A) (black) which shows significantly reduced amplitudes of both the amide I band and signals from side chain groups around 1689 cm^{-1} and over the 1610−1580 cm^{-1} region. (B) pB − pG infrared spectrum of PYP in $P6_3$ crystals. The pB_{355} − pG_{446} spectrum of wt-PYP in solution (gray) is presented in both panels A and B for comparison; the dashed lines represent $\Delta A = 0$.

dimensional structure of proteins in atomic detail, and has played a crucial role in understanding the molecular mechanism of protein function. Time-resolved X-ray crystallography has recently become possible (*22*, *29*), opening a novel field of investigation on the structural changes during protein function. The X-ray structure of pB was determined using millisecond time-resolved X-ray crystallography on $P6_3$ PYP crystals (*29*). The pB structure formed in $P6_3$ crystals was found to be very similar to that of pG_{446}, in contrast with other observations on pB_{355} in aqueous solution using a range of techniques (*27*, *28*). To resolve this dispute, we performed time-resolved FTIR spectroscopy on wt-PYP in $P6_3$ crystals. The pB − pG spectrum of PYP in $P6_3$ crystals (Figure 3B) reveals no changes in the protein backbone (amide I), and dramatically reduced changes in the side chain groups (1610−1560 cm^{-1}). Therefore, the structure of the putative signaling state pB_{355} is not developed in $P6_3$ crystals. Furthermore, a positive band of COOD stretching is observed at 1757 cm^{-1}, indicating the presence of protonated Glu46 in a highly hydrophobic pocket in pB in $P6_3$ crystals.

Our results demonstrate that the structure of the pB-like state in PYP $P6_3$ crystals is very different from that of the pB_{355} state in PYP solution. In addition, the pB to pG transition is approximately 10 times faster in $P6_3$ crystals

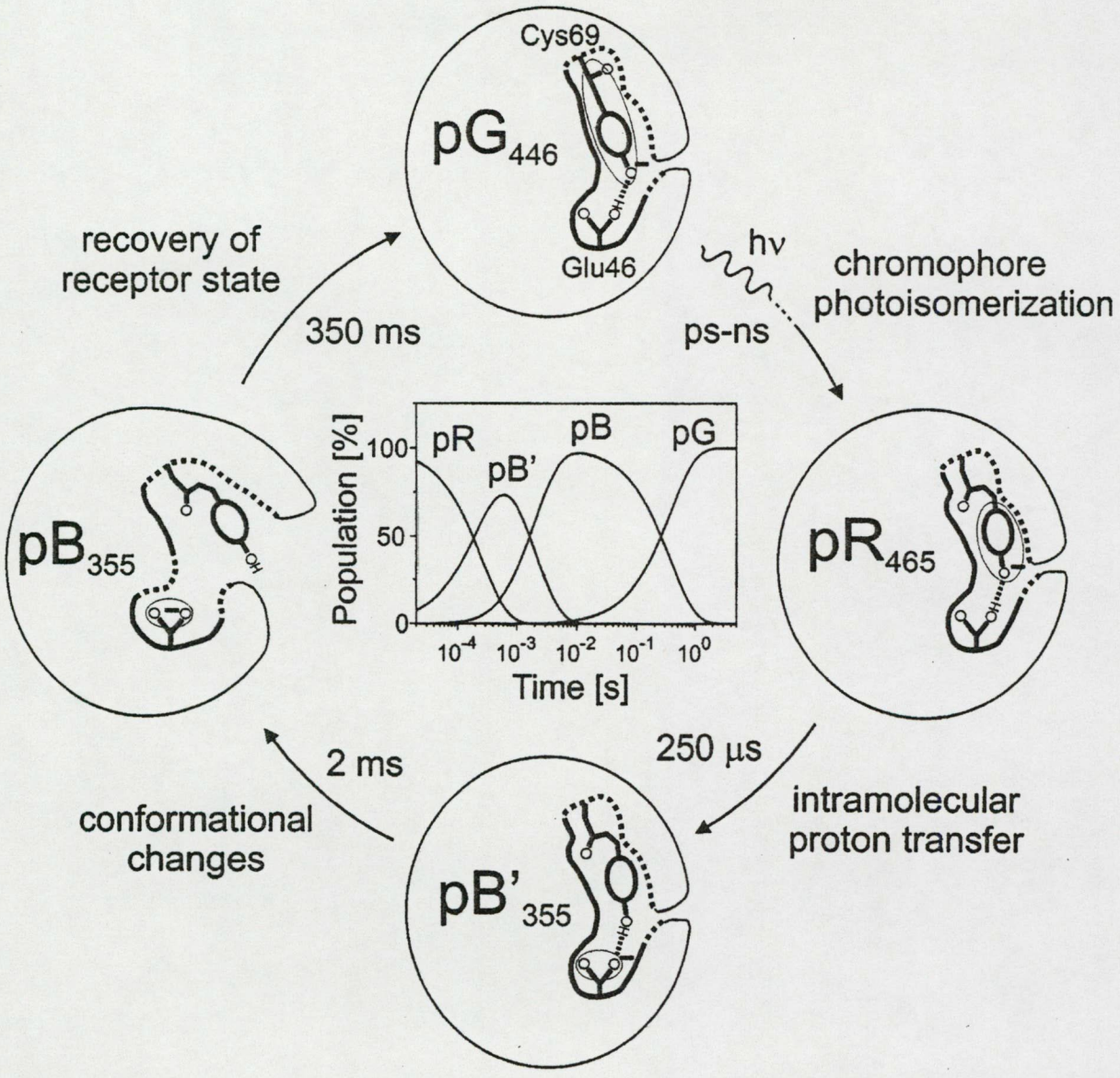

FIGURE 4: PYP photocycle and a molecular mechanism for PYP activation. Three intermediates (pR_{465}, pB'_{355}, and pB_{355}) of the PYP photocycle are depicted. Their population accumulations are shown in the inset. The electrostatic properties of the binding pocket for the chromophore and Glu46 are denoted using thick dashed lines for high-dielectric environments, thick solid lines for low-dielectric environments, and thin solid lines for unspecified dielectric environments. The charge delocalizations are qualitatively represented by shaded ovals.

than in solution, in agreement with kinetic measurement of single $P6_3$ crystals (*15*). Therefore, the photocycle of PYP is both structurally and kinetically different between the $P6_3$ crystal state and the solution state.

The large differences between the pB states in crystals and in aqueous solution raise the question of which pB state is active in intact cells. This question will be discussed here in terms of protein concentration, water content, and lattice contacts. The total protein concentration in the cytoplasm of bacteria is ~50 mg/mL. In $P6_3$ crystals, the PYP concentration is approximately 650 mg/mL. In comparison, the PYP concentration of our FTIR samples is 140 mg/mL (10 mM), and is therefore closer to physiological conditions. In terms of water content, PYP is a highly water soluble protein. PYP molecules in our FTIR samples are fully hydrated with 4800 water molecules per PYP. When the hydration level of proteins is reduced to ~350 water molecules per PYP, the large structural changes during pB formation are fully suppressed (*27*). The hydration level in $P6_3$ crystals is ~500 H_2O molecules per PYP, only slightly higher than 350 H_2O molecules per PYP. This partial dehydration can reduce the extent of structural changes in $P6_3$ crystals. Finally, the inhibition of large conformational changes may be caused by restraints imposed by the large number of protein−protein contacts that form the $P6_3$ crystal lattice (58 contacts per PYP) (*30*). In general, such lattice contacts may prevent the full development of conformational changes during the functional cycle of a protein (*31*). Therefore, the structure of pB_{355} formed in aqueous solution at room temperature and neutral pH of our FTIR samples is expected to be closer to that of the putative signaling state under physiological conditions than the pB structure formed

in crystals. It is possible, however, that interactions between PYP and its signal transducer may affect the structure of the pB state in the living cell.

We show that time-resolved FTIR spectroscopy is a powerful technique for testing the transient structures of proteins in solution and in crystals. Prior to this work, only one time-resolved FTIR spectroscopic study of protein crystals has been reported (*32*) on bacteriorhodopsin (bR), a membrane protein for the light-driven proton pump. Structural changes of bR during its proton pumping photocycle are very similar in both membrane and crystal states. Since bR molecules form two-dimensional crystals in native purple membranes, no large conformational changes are present even in the native state. It is therefore not too unexpected that the structural changes in the three-dimensional crystals of bR molecules are similar to those in the two-dimensional native crystals. In contrast, PYP is a water soluble photoreceptor protein, and large conformational changes can well be associated with signal relay via intermolecular interactions. In conclusion, one must be cautious in drawing conclusions regarding the functional mechanism of proteins based on time-resolved X-ray crystallography prior to direct experimental testing on the structural developments of a protein during its functional process in both crystal and solution states.

A Molecular Mechanism for PYP Activation. We propose the following molecular mechanism for receptor activation in PYP, as depicted in Figure 4. In the receptor state, pG_{446}, a built-in structural fault for a protein quake is present at the photoactive site, consisting of the negatively charged phenolic group of the pCA chromophore and the protonated carboxylic group of Glu46. These two groups exhibit anomalously shifted p*K*s in opposite directions. The abnormal charge state of the pCA is stabilized by intricate hydrogen bonding interactions, one counter charge from Arg52, and various hydrophilic interactions at the pCA binding pocket (*14*) (Figure 2). The neutral charge state of Glu46 is enforced by a highly hydrophobic binding pocket. In pR_{465}, chromophore photoisomerization (*13*, *33*) dramatically increases the proton affinity of the phenolic oxygen in pCA so that it abstracts a proton from Glu46 to form pB'_{355}. The origin of the enhanced proton affinity of the chromophore in pR_{465} is beyond the scope of this work. The pR_{465} to pB'_{355} transition involves localized, direct proton transfer from Glu46 to the chromophore, without changes in global protein conformation. The resulting negative charge on Glu46 is embedded in a highly hydrophobic cavity in pB'_{355}, and is therefore energetically unstable. As this charged group is searching for a more charge-friendly surrounding (higher-dielectric areas), it triggers and drives a large-amplitude protein quake. The epicenter of the protein quake is located at the hydrophobic active site where a new buried charge, COO^- of Glu46, is formed via intramolecular proton transfer to the anionic pCA chromophore. The large-amplitude protein quake takes place during the pB'_{355} to pB_{355} transition, leading to the formation of the putative signaling state pB_{355}. The actual time for a protein quake to take place in individual PYP molecules is not 2 ms, the time constant of the pB'_{355} to pB_{355} transition for an ensemble of many PYP molecules, but much faster than that, on the order of picosecond to nanosecond time scales (*34*). The decisive role of Glu46 in driving a large-amplitude protein quake and PYP activation is further supported by the fact that Glu46 is conserved within the PYP family (*35*). This mechanism for protein quakes is not restricted to PYP, but may play roles during the functioning of other receptor proteins and nonreceptor proteins that require large conformational changes.

ACKNOWLEDGMENT

We thank S. Anderson and P. A. Croonquist for the preparation of $P6_3$ PYP crystals and thank B. Nie, J. Wang, and B.-C. Lee for technical assistance. We also thank D. Rousseau and R. H. Austin for valuable comments.

SUPPORTING INFORMATION AVAILABLE

List of dielectric constants for various polar and nonpolar solvents and four figures showing the assignment of a pCA-ring vibration mode around 1500 cm^{-1}, the assignment of the 1689 cm^{-1} band to a ND-containing side chain, vibrational modes of the pCA methyl ester, and normalization of the pB − pG spectrum of the E46Q mutant. This material is available free of charge via the Internet at http://pubs.acs.org.

REFERENCES

1. Honig, B., and Nicholls, A. (1995) *Science 268*, 1144−1149.
2. Honig, B., and Yang, A.-S. (1995) *Adv. Protein Chem. 46*, 27−58.
3. Ansari, A., Berendzen, J., Bowne, S. F., Frauenfelder, H., Iben, L. E., Sauke, T. B., Shyamsunder, E., and Young, R. D. (1985) *Proc. Natl. Acad. Sci. U.S.A. 82*, 5000−5004.
4. Pellequer, J. L., Wager-Smith, K. A., Kay, S. A., and Getzoff, E. D. (1998) *Proc. Natl. Acad. Sci. U.S.A. 95*, 5884−5890.
5. Taylor, B. L., and Zhulin, I. B. (1999) *Microbiol. Mol. Biol. Rev. 63*, 479−506.
6. Meyer, T. E., Yakali, E., Cusanovich, M. A., and Tollin, G. (1987) *Biochemistry 26*, 418−423.
7. Sprenger, W. W., Hoff, W. D., Armitage, J. P., and Hellingwerf, K. J. (1993) *J. Bacteriol. 175*, 3096−3104.
8. Jiang, Z., Swem, L. R., Rushing, B. G., Devanathan, S., Tollin, G., and Bauer, C. E. (1999) *Science 285*, 406−409.
9. Hoff, W. D., Dux, P., Hard, K., Devreese, B., Nugteren-Roodzant, I. M., Crielaard, W., Boelens, R., Kaptein, R., van Beeumen, J., and Hellingwerf, K. J. (1994) *Biochemistry 33*, 13959−13962.
10. Baca, M., Borgstahl, G. E., Boissinot, M., Burke, P. M., Williams, D. R., Slater, K. A., and Getzoff, E. D. (1994) *Biochemistry 33*, 14369−14377.
11. Hoff, W. D., van Stokkum, I. H., van Ramesdonk, H. J., van Brederode, M. E., Brouwer, A. M., Fitch, J. C., Meyer, T. E., van Grondelle, R., and Hellingwerf, K. J. (1994) *Biophys. J. 67*, 1691−1705.
12. Ujj, L., Devanathan, S., Meyer, T. E., Cusanovich, M. A., Tollin, G., and Atkinson, G. H. (1998) *Biophys. J. 75*, 406−412.
13. Xie, A., Hoff, W. D., Kroon, A. R., and Hellingwerf, K. J. (1996) *Biochemistry 35*, 14671−14678.
14. Borgstahl, G. E., Williams, D. R., and Getzoff, E. D. (1995) *Biochemistry 34*, 6278−6287.
15. Ng, K., Getzoff, E. D., and Moffat, K. (1995) *Biochemistry 34*, 879−890.
16. Jackson, J. D. (1999) *Classical Electrodynamics*, 3rd ed., John Wiley & Sons, New York.
17. Hage, W., Kim, M., Frei, H., and Mathies, R. A. (1996) *J. Phys. Chem. 100*, 16026−16033.
18. Rothschild, K. J. (1992) *J. Bioenerg. Biomembr. 24*, 147−167.
19. Venyaminov, S. U., and Kalnin, N. N. (1990) *Biopolymers 30*, 1259−1271.
20. Arrondo, J. L., Muga, A., Castresana, J., and Goñi, F. M. (1993) *Prog. Biophys. Mol. Biol. 59*, 23−56.

21. Venyaminov, S. Y., and Kalnin, N. N. (1990) *Biopolymers 30*, 1243−1257.
22. Perman, B., Srajer, V., Ren, Z., Teng, T., Pradervand, C., Ursby, T., Bourgeois, D., Schotte, F., Wulff, M., Kort, R., Hellingwerf, K., and Moffat, K. (1998) *Science 279*, 1946−1950.
23. Nakanishi, K., and Solomon, P. M. (1977) *Infrared Absorption Spectroscopy*, Holden-Day, San Francisco.
24. Genick, U. K., Devanathan, S., Meyer, T. E., Canestrelli, I. L., Williams, E., Cusanovich, M. A., Tollin, G., and Getzoff, E. D. (1997) *Biochemistry 36*, 8−14.
25. Nagle, J. F., and Mille, M. (1981) *J. Chem. Phys. 74*, 1367−1372.
26. Mihara, K., Hisatomi, O., Imamoto, Y., Kataoka, M., and Tokunaga, F. (1997) *J. Biochem. 121*, 876−880.
27. Hoff, W. D., Xie, A., Van Stokkum, I. H., Tang, X. J., Gural, J., Kroon, A. R., and Hellingwerf, K. J. (1999) *Biochemistry 38*, 1009−1017.
28. Rubinstenn, G., Vuister, G. W., Mulder, F. A., Dux, P. E., Boelens, R., Hellingwerf, K. J., and Kaptein, R. (1998) *Nat. Struct. Biol. 5*, 568−570.
29. Genick, U. K., Borgstahl, G. E., Ng, K., Ren, Z., Pradervand, C., Burke, P. M., Srajer, V., Teng, T. Y., Schildkamp, W., McRee, D. E., Moffat, K., and Getzoff, E. D. (1997) *Science 275*, 1471−1475.
30. Van Aalten, D. M. F., Crielaard, W., Hellingwerf, K. J., and Joshua-Tor, L. (2000) *Protein Sci. 9*, 64−72.
31. Makinen, M. W., and Fink, A. L. (1977) *Annu. Rev. Biophys. Bioeng. 6*, 301−343.
32. Heberle, J., Buldt, G., Koglin, E., Rosenbusch, J. P., and Landau, E. M. (1998) *J. Mol. Biol. 281*, 587−592.
33. Genick, U. K., Soltis, S. M., Kuhn, P., Canestrelli, I. L., and Getzoff, E. D. (1998) *Nature 392*, 206−209.
34. Frauenfelder, H., and Wolynes, P. G. (1985) *Science 229*, 337−345.
35. Kort, R., Hoff, W. D., Van West, M., Kroon, A. R., Hoffer, S. M., Vlieg, K. H., Crielaand, W., Van Beeumen, J. J., and Hellingwerf, K. J. (1996) *EMBO J. 15*, 3209−3218.

BI002449A